

Atmospheric Tests of Trailing-Edge Aerodynamic Devices

L. Scott Miller
Wichita State University
Wichita, Kansas

Gene A. Quandt
Wind Turbine Engineering Consultant
Seattle, Washington

Steve Huang
Wichita State University
Wichita, Kansas



National Renewable Energy Laboratory
1617 Cole Boulevard
Golden, Colorado 80401-3393
A national laboratory of the U.S. Department of Energy
Managed by the Midwest Research Institute
for the U.S. Department of Energy
Under Contract No. DE-AC36-83CH10093

Atmospheric Tests of Trailing-Edge Aerodynamic Devices

L. Scott Miller
Wichita State University
Wichita, Kansas

Gene A. Quandt
Wind Turbine Engineering Consultant
Seattle, Washington

Steve Huang
Wichita State University
Wichita, Kansas

NREL technical monitor: Paul Migliore



National Renewable Energy Laboratory
1617 Cole Boulevard
Golden, Colorado 80401-3393
A national laboratory of the U.S. Department of Energy
Managed by Midwest Research Institute
for the U.S. Department of Energy
under contract No. DE-AC36-83CH10093

Work performed under Subcontract No. XAX-5-15217-01

January 1998

NOTICE

This report was prepared as an account of work sponsored by an agency of the United States government. Neither the United States government nor any agency thereof, nor any of their employees, makes any warranty, express or implied, or assumes any legal liability or responsibility for the accuracy, completeness, or usefulness of any information, apparatus, product, or process disclosed, or represents that its use would not infringe privately owned rights. Reference herein to any specific commercial product, process, or service by trade name, trademark, manufacturer, or otherwise does not necessarily constitute or imply its endorsement, recommendation, or favoring by the United States government or any agency thereof. The views and opinions of authors expressed herein do not necessarily state or reflect those of the United States government or any agency thereof.

Available to DOE and DOE contractors from:
Office of Scientific and Technical Information (OSTI)
P.O. Box 62
Oak Ridge, TN 37831
Prices available by calling (423) 576-8401

Available to the public from:
National Technical Information Service (NTIS)
U.S. Department of Commerce
5285 Port Royal Road
Springfield, VA 22161
(703) 487-4650



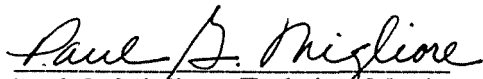
Foreword

The Wind Technology Division of the National Renewable Energy Laboratory (NREL) is conducting exploratory research on aerodynamic devices that are intended to enhance wind-turbine rotor performance and attenuate structural loads. Desired properties of these devices include simplicity, reliability, maintainability, low cost and fail-safe design. Initial efforts have focused on the use of trailing-edge aerodynamic brakes for overspeed protection. Long-term efforts will address more aggressive and innovative strategies that have the potential to significantly advance the state of the art.

The first two research projects proceeded in parallel, with considerable interaction between the principal investigators: Subcontract No. TAD-3-13400 entitled "Wind Turbine Trailing-Edge Aerodynamic Brake Design" performed by Gene A. Quandt, and Subcontract No. XAD-3-133365 entitled "Aerodynamic Devices for Wind Turbine Performance Enhancement" performed by Wichita State University (WSU).

The WSU Phase-1 Report discussed the configurations studied and the attempts to identify promising alternatives through the analysis of the wind tunnel test data. The Phase-2 Report presented wind-tunnel results for "spoiler-flaps" of 30%, 40% and 50% chord; for various leading-edge lip extensions; for different venting arrangements; and for different device hinge locations. Gene Quandt's subcontract report, No. TP-441-7389, focused on aerodynamic and structural design, and included preliminary design calculations for a centrifugally-actuated aerodynamic brake.

As is often the case with exploratory research, these projects spawned additional follow-on studies. Wind-tunnel tests were conducted at Ohio State University (OSU) in which a pressure-tapped S809 airfoil model was tested with three trailing-edge devices: the spoiler-flap, a plain flap ("unvented aileron") and a vented plain flap ("vented aileron"). In Subcontract No. XAX-5-15217-0 entitled "Investigation of Trailing-Edge Aerodynamic Brakes", rotating-blade tests of these same configurations were conducted at the National Wind Technology Center (NWTC) with the goal of quantifying the effects of unsteadiness, blade rotation and aspect ratio, so that corrections might be applied to wind-tunnel test data for use by wind-turbine designers in the future. The results of that effort are contained in the present report.


Paul G. Migliore, Technical Monitor

Preface

The information presented in this report represents a great deal of work and time. It is the product of a team effort, in every sense of the phrase.

Paul Migliore and many others at the National Renewable Energy Laboratory (NREL) National Wind Technology Center (NWTC) arranged for us to conduct the atmospheric tests. As far as the authors are aware, this investigation was the first where non-NREL personnel conducted their experiments independently using a NWTC turbine. The exercise was valuable, enlightening, and pleasurable. Lee Fingersh and Dave Jager, in particular, provided extensive training and technical guidance during the process of preparing for and conducting the actual tests. Without their valuable help we would not have succeeded.

Art Porter at Wichita State University's (WSU's) Engineering Research Machine Shop, deserves special recognition. He worked closely with all involved in designing the control mechanisms, modifying the turbine blades, building the various parts, and assembling the components. Art is an engineering machinist truly worth his weight in gold. His long hours of work resulted in test blades and devices that worked as designed. Art's attention to quality and detail will pay dividends in many ways for years to come.

Rick DeMoss, Ihssane Mounir, Tom Wayman, and Ryan Schaefer, all from WSU, also helped a great deal on the project. Rick quickly mounted and repaired strain-gages as fast as we could break them, with a smile on his face virtually every time. Ihssane, Tom, and Ryan learned more working on the project than they ever could have as students in a classroom. Their enthusiasm and commitment to learning will continue to serve them well in the future.

A debt of gratitude is extended to the many people that reviewed this report during its preparation. Their positive input and commentary was most welcome and helped to assure that a long and difficult process was completed as effectively as possible. I'm sure that the process was challenging and time consuming for the reviewers. Thank you, sincerely, for your help.

NREL and the US Department of Energy are to be commended for their support of projects such as this one. We sincerely hope that the results are beneficial to all involved and interested.

Summary

An experiment was conducted at the National Renewable Energy Laboratory's (NREL's) National Wind Technology Center (NWTC) using an instrumented horizontal-axis wind turbine that incorporated variable-span, trailing-edge aerodynamic brakes. The goal of the investigation was to directly compare results with (infinite-span) wind tunnel data and to provide information on how to account for device span effects during turbine design or analysis. Comprehensive measurements were used to define effective changes in the aerodynamic and hinge-moment coefficients, as a function of angle of attack and control deflection, for three device spans (7.5%, 15%, and 22.5%) and configurations (Spoiler-Flap, vented sileron, and unvented aileron). Differences in the lift and drag behavior are most pronounced near stall and for device spans of less than 15%. Drag performance is affected only minimally (about a 30% reduction from infinite-span) for 15% or larger span devices. Interestingly, aerodynamic controls with vents or openings appear most affected by span reductions and three-dimensional flow.

Contents

	Page
Nomenclature	1
Introduction	2
Previous Related Work	3
Investigation Goals	3
Experimental Apparatus and Method	4
Blade Modifications	4
Test Turbine	9
Test Configuration	9
Test Procedure	13
Test Reynolds Numbers	13
Data Reduction	13
Aerodynamic Coefficients	14
Hinge-moments	16
Presentation of Force-Coefficient Results	17
Spoiler-Flap	17
Vented Aileron	21
Unvented Aileron	24
Discussion of Force Coefficient Results	27
Span Effects and Lift	27
Span Effects and Drag	28
Uncertainty Analysis	30
Hinge-Moment Results	32
Conclusions	36
References	37

Nomenclature

c	Airfoil or blade chord, including the device
c_c	Trailing-edge device chord
L	Section lift, per unit span, acting perpendicular to approach flow direction
D	Section drag, per unit span, acting parallel to approach flow direction
M_E	Blade root flap moment
M_F	Blade root edgewise moment
M_h	Trailing-edge device hinge-moment; trailing edge down is positive
C_l	Section lift-force coefficient, $L/(qc)$
C_d	Section drag-force coefficient, $D/(qc)$
C_n	Section normal-force coefficient, $N/(qc)$
C_s	Section suction-force coefficient, $C_l \sin \alpha - C_d \cos \alpha$
Cm_h	Trailing-edge device hinge-moment coefficient, $M_h/(qSc_c)$
q	Dynamic pressure at device mid-span, $0.5\rho V^2$
r	Radius to device mid-span
R_c	Reynolds number, Vrc/μ
S	Blade area over which trailing-edge device is active, $\Delta r c$
V_{wind}	Time average wind velocity
α	Airfoil angle of attack; nose up is positive
β	Blade pitch angle
Δr	Trailing-edge device span
δ	Trailing-edge device deflection angle
λ	Ratio between finite- and infinite-span drag values
μ	Absolute viscosity of air
Ω	Rotor rotational speed
ρ	Mass density of air

Introduction

Mechanical brakes are common components on many wind turbines. These brakes are effective at holding a stopped rotor and in many cases at stopping a turning rotor. However, under severe wind conditions or as a result of generator load loss, mechanical brakes may prove to be inadequate, leading to overspeed and turbine damage. Therefore a redundant means of controlling the rotor is desirable, one that is lightweight, simple in design, and reliable. In addition, the new brake should offer a means of turbine control, including power modulation or active load alleviation.

Aerodynamic techniques such as tip brakes and direct blade pitch (full-span or partial-span) have been used to adjust rotor torque on a number of horizontal-axis wind turbines. Unfortunately, the utility, effectiveness, and reliability of these methods have not always been as desired, and there is still a need for efficient rotor control. Tip-mounted, trailing-edge aerodynamic control surfaces are one possible alternative. Because of their rough resemblance to similar controls used on airplanes, these aerodynamic-control devices are sometimes referred to as "ailerons." However, their function is to adjust loads over the primary torque producing area of the wind turbine rotor blade. Because they are small in size, relative to the entire rotor, there is potential for simple and effective rotor torque control.

To be effective in this application, the control device must adjust the airfoil's flow character so as to reduce or even reverse the normally pro-rotational torque of the entire rotor. This requirement for turbine braking is demanding, especially in light of the turbine blade's inherent function of generating high torque during typical power generation periods. Aerodynamically, the trailing-edge control device must greatly reduce the lift and increase the drag over a large angle-of-attack range.

It is common to measure the aerodynamic potential of a specific device by measuring or predicting the suction-force coefficient (C_s). As the following equation shows, the suction-force coefficient depends on the section lift and drag coefficients and is equal to the negative of the chord-force coefficient.

$$C_s = C_l \cos \alpha - C_d \sin \alpha$$

The suction-force is best thought of as the section aerodynamic force that aligns itself most closely to the rotor plane of rotation in the torque direction. During normal power production periods the suction coefficient is positive. When rotor braking is needed the suction coefficient must be negative, and of a sufficient magnitude to overcome the driving torque produced by the remainder of the rotor.

For more moderate rotor torque or power output control, the aerodynamic devices can be deflected by smaller amounts. These deflections can be used to increase or decrease the rotor torque so that power output becomes more constant over a wider wind speed range. This application is commonly known as "power modulation." Interestingly, other benefits can be realized through small device deflections of this type as well.

Wind turbines operate in a very unsteady environment and they respond in a dynamic way. As a result, fatigue and structural resonance are significant concerns for a turbine designer, manufacturer, and operator, aerodynamic devices offer the potential to address this problem. By rapidly deflecting the aerodynamic control devices, as a function of azimuth location and condition, they can be used to limit rotor blade loads. Helicopters (Seddon 1990 and Prouty 1988) and fixed-wing aircraft (Taylor 1974) have both been tested with active aerodynamic control methods for load alleviation. Simplified, more mature techniques are rapidly evolving; it is possible they will be widely used on aircraft and, potentially, on wind turbines, in the very near future.

Previous Related Work

Researchers have been working to develop, evaluate, and apply aerodynamic devices for rotor braking. Power modulation and active control (or load alleviation) are, however, quickly emerging as high-priority applications. Investigators have focused on identifying device configurations that produce reasonable braking capabilities, subject to simplicity of construction, ease of actuation, and operational reliability considerations. Indeed, a number of different configurations have been evaluated in wind tunnel tests (Quandt 1994, Miller 1995 and 1996, Griffin 1996, Ramsay, Janiszewska, and Gregorek 1996). Comprehensive databases for each configuration exist and are available for designers. However, there have been a number of questions raised concerning the utility and accuracy of the wind tunnel data. Most significantly, the data have been almost exclusively for two-dimensional (i.e., infinite-span) flow cases and for lower-than-typical Reynolds numbers.

The flow through a rotor especially near the tip, is anything but two-dimensional. A significant amount of shed vorticity exists and its effect on the rotor tip flow field could be significant. In addition, the resulting flow velocity and dynamic pressure vary, both along the blade span and with time. Significant Reynolds number differences suggest variances in the boundary layer development and behavior, thus potentially resulting in aerodynamic performance changes. Unfortunately, wind tunnel testing at higher Reynolds numbers has been very challenging, as it has been for the aerospace industry. In summary, turbine designers either need more representative aerodynamic information, or they need to understand how to better apply the existing data.

Investigation Goals

In light of the above-discussed needs and problems, an investigation was undertaken to further evaluate aerodynamic control devices for turbine braking applications, and potentially for power modulation and active control. An actual rotor was modified and tested, by the authors, in an atmospheric environment and on an instrumented turbine at the National Renewable Energy Laboratory's (NREL) National Wind Technology Center (NWTC). Three aerodynamic-control devices, each of variable span, were evaluated. Blade loads and turbine conditions were measured and used to identify the performance of each device in a rotating, unsteady, three-dimensional environment. The resulting data are compared to two-dimensional infinite-span data obtained from wind tunnel tests for the same device configurations (Ramsay, Janiszewska, and Gregorek 1996). The following is an overview of the specific goals of this work:

- 1) Perform atmospheric, rotating-frame tests at the NWTC:
 - a) Modify supplied turbine rotor blades to incorporate three device configurations and spans
 - b) Include instrumentation for device hinge-moment measurements
 - c) Deliver the blades to the NWTC and "certify" them for use on an instrumented wind turbine
 - d) Receive safety and operational training necessary to conduct the tests with minimal supervision
 - e) Organize and conduct the tests at the NWTC.
- 2) Analyze and compare results to similar two-dimensional wind tunnel data:
 - a) Reduce and analyze the resulting data
 - b) Compare information with supplied two-dimensional wind tunnel data
 - c) Develop, if possible, prediction or correction methods for the two-dimensional data
 - d) Offer suggestions for future research, testing, and aerodynamic control device applications.

Experimental Apparatus and Method

The atmospheric test were performed using the NWTC's Grumman 20 kilowatt (kW), horizontal-axis wind turbine. This machine was previously labeled and is commonly known as the Combined Experiment Rotor (CER) (Butterfield 1992). It was used for other purposes before, but it suited the current application because of its extensive instrumentation provisions.

The CER turbine is normally equipped with constant-chord twisted blades of 5.0-meter span. Untwisted blades, of the same span and 0.46-meter chord, were used for the current investigation. The airfoil profile was constant (S809 series). The machine is normally free to yaw and operates in a down wind configuration.

Blade Modifications

Three test blades were delivered to the Wichita State University (WSU) National Institute for Aviation Research (NIAR) Engineering Research Machine Shop for modification to incorporate the aerodynamic-control devices. The outboard trailing edge ($\approx 45\%$ -chord) of each fiberglass blade was cut out for device installation (see Figure 1). The spars were reinforced and machined to a consistent reference surface so as to accept each device. The control mounts, supports, and device deflection mechanisms had to be designed such that they were strong, stiff, lightweight, and reliable. Relatively easy configuration changes, pivot-point movements, and device deflection adjustments were also required, because working in a man-lift during testing was anticipated. In addition, provisions for a strain-gage apparatus were included to obtain hinge-moments for each configuration. Many of these constraints and requirements are representative of those that a turbine manufacturer must face when designing and building a marketable machine using similar aerodynamic-control devices. Considerable time and care were required to design and modify the blades. All work was performed using 3-D Computer-Aided Design software and Computer Numerically Controlled milling machines.

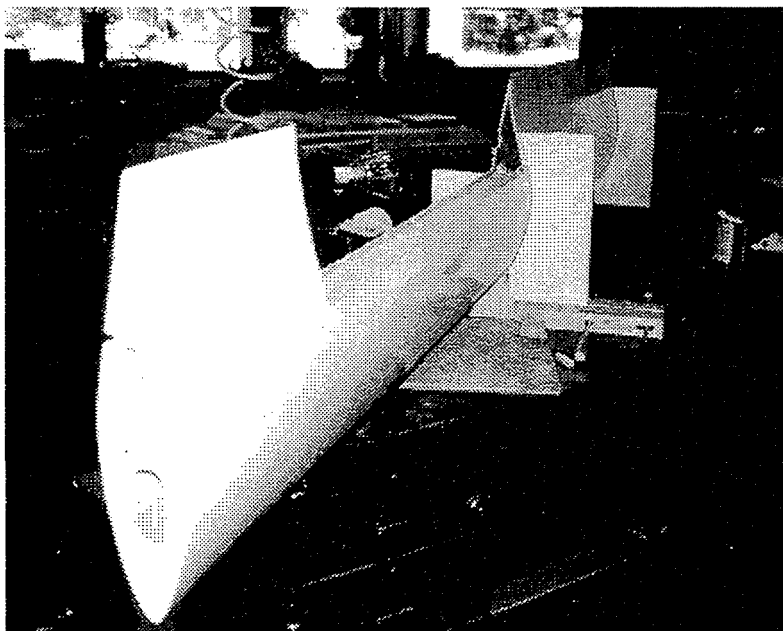


Figure 1. Photograph showing rotor cut-out for aerodynamic control installation (in WSU machine shop).

The weight penalty incurred as a result of the blade modifications was about 50 pounds, above an initial blade weight of about 75 pounds. It is critical to note that these numbers are for the variable-span (i.e., research) mechanism installed. Actual weight penalties for production turbine blades will be notably less, at least a third of 50 pounds, because an operational turbine will not use variable-span capabilities.

As previously mentioned, provisions for three different device spans were included. Each segment had a length equal to 7.5% of the blade span and it could be deflected independently or together with the others, thus allowing a number of combinations for evaluation (see Figures 2 and 3). Mounting hardware and instrumentation was fully accessible once the devices were manually deflected to an extreme position. Leading-edge and cove pieces were changed out and the hinge points were moved in order to generate each specific aerodynamic control shape or configuration.

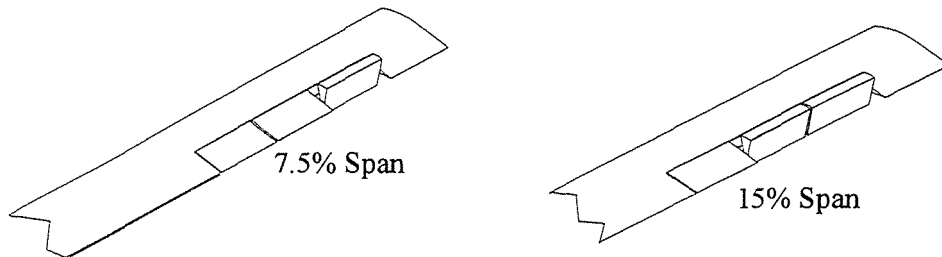


Figure 2. Diagrams illustrating aerodynamic device deflections for two different spans.

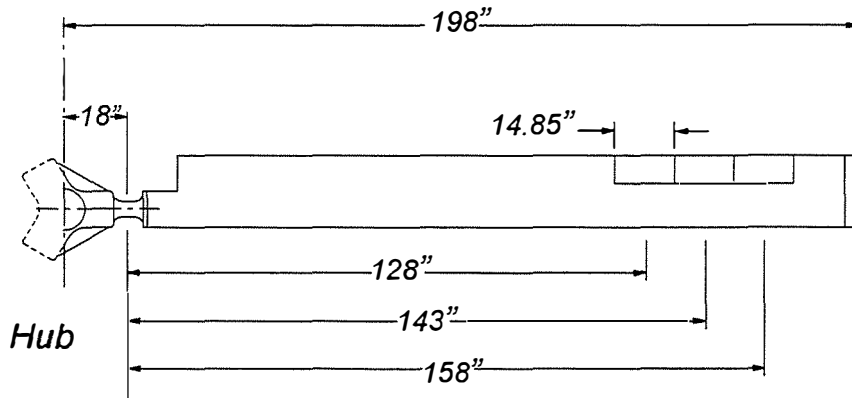


Figure 3. Diagram showing blade dimensions, device spans, and centerline locations (in inches).

Forty-percent chord (i.e., 0.40c) spoiler-flap, vented aileron, and unvented aileron trailing-edge aerodynamic devices were examined in the investigation, as shown in Figure 4. The spoiler-flap and vented aileron use the same pivot-point and torque-tube mechanism (located on the chordline, at the 80%-chord location) for hinge-moment measurements. Note that the spoiler-flap trailing-edge is designed to move primarily downward, whereas the other two configurations are designed to move trailing edge up. Small deflections in the other directions are possible for power modulation applications, however. The unvented aileron control surface pivoted about a point next to the surface (at the 62%-chord location) and tension-compression links were used to obtain hinge-moment data.

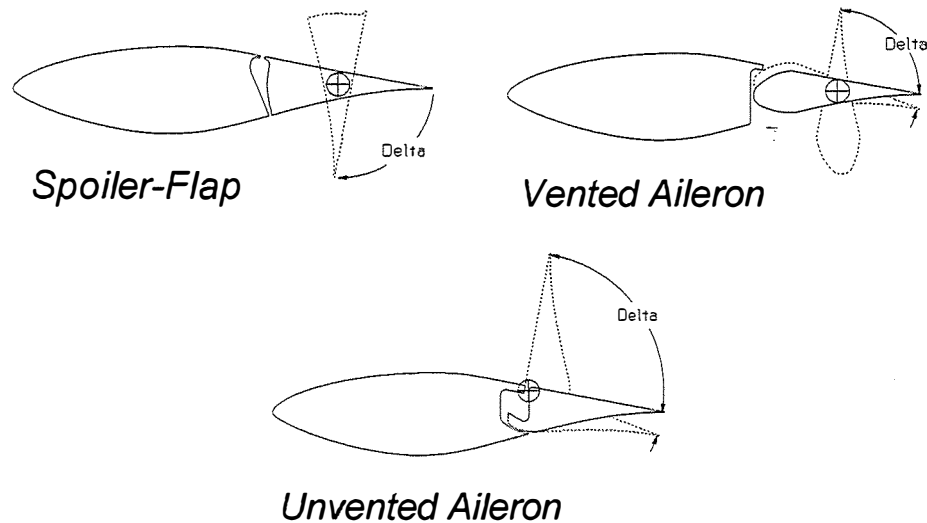


Figure 4. The three 40%-chord aerodynamic devices examined, as installed on 0.46-meter chord S809 airfoil.

Design of a simple and accurate hinge-moment measurement apparatus proved extremely challenging, especially in light of the need to accommodate various device configurations and spans. The integral-mount and torque-tube mechanism worked quite well for the spoiler-flap and vented aileron. Unfortunately, the unvented aileron tension-compression link proved more troublesome. Binding of the tension-compression linkages, most likely in the span-wise direction, made hinge-moment readings for this control configuration less reliable. Problems of this sort were considered early during the design and blade modification process, but a reasonable solution was not identified (without using large ball bearings). It was expected that the hinge-moment behavior of the unvented aileron configuration would be "fairly predictable," as a result of its basic form (i.e., it is much like a simple flap). The hinge-moment character of the other two devices was expected to be more complicated. These factors made it more critical to focus on the reliable measurement of hinge-moments for the spoiler-flap and vented aileron. Figure 5 shows a drawing of the torque-tube and compression-link apparatus, around which the aerodynamic control surfaces would fit.

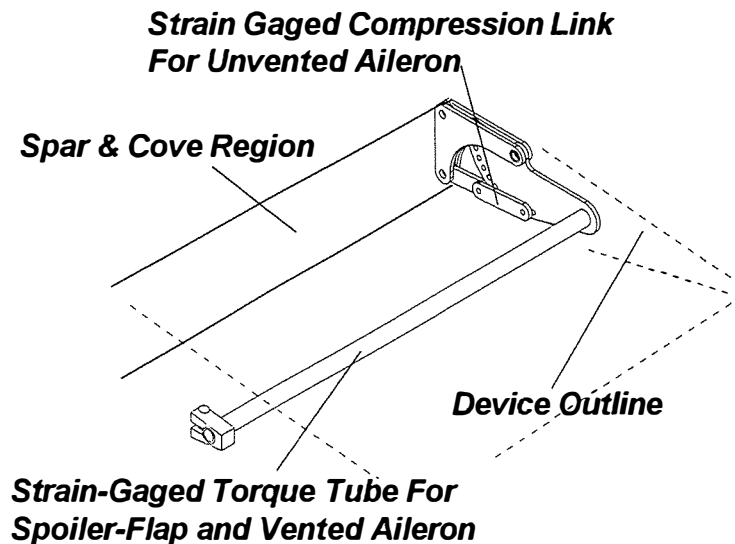


Figure 5. Drawing of torque-tube and tension-link mechanism used for hinge-moment measurements.

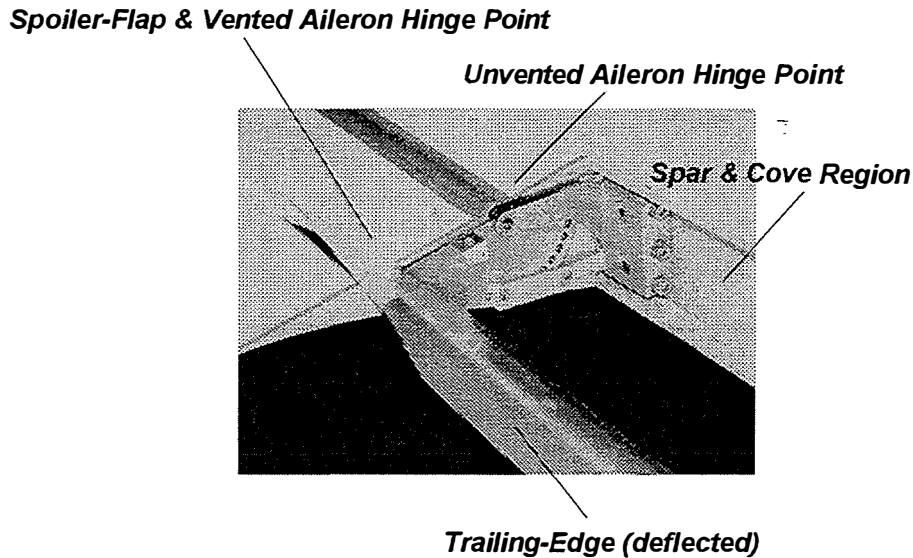


Figure 6. Close-up photograph of control installation and apparatus for spoiler-flap and vented aileron configurations.

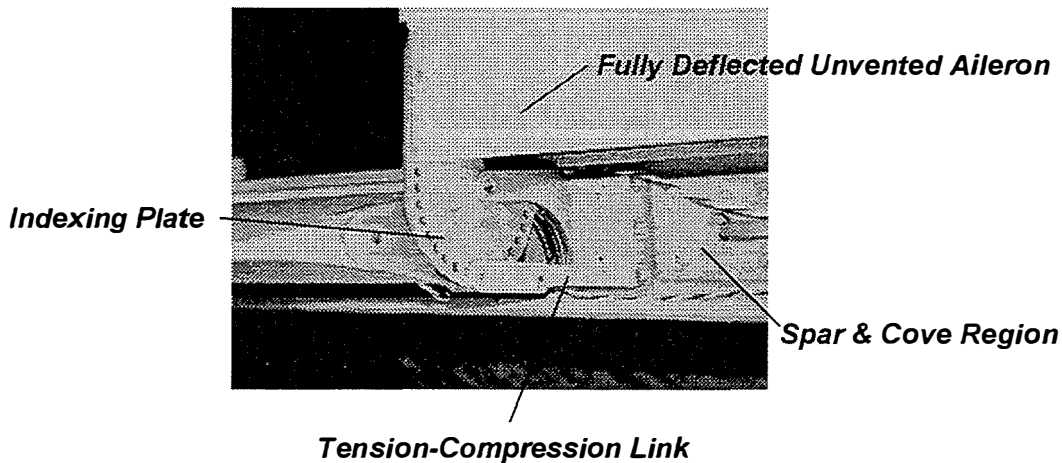


Figure 7. Close-up photo of unvented aileron installation and apparatus.

The spoiler-flap and vented aileron deflection angles were set by rotating the devices about the torque-tube assembly until the desired value was obtained, as indicated by a close-fitting template. Unvented aileron deflection angles were set by moving an indexing plate to one of eighteen different holes, thus allowing five degree deflection increments from zero to ninety degrees (see Figures 6 and 7).

Control leading-edge and cove pieces were made to allow for the testing of the three different configurations. As was the case for previous wind tunnel models (Miller 1995 and 1996), these parts simply bolted into position on the common blade trailing edge and cove so as to create the geometry desired. Most of the instrumentation and device hinge mechanisms were also covered in the process. Enough parts for three rotor blades were produced and carefully balanced for installation as desired. Figure 8 shows some of the leading-edge and cove pieces.

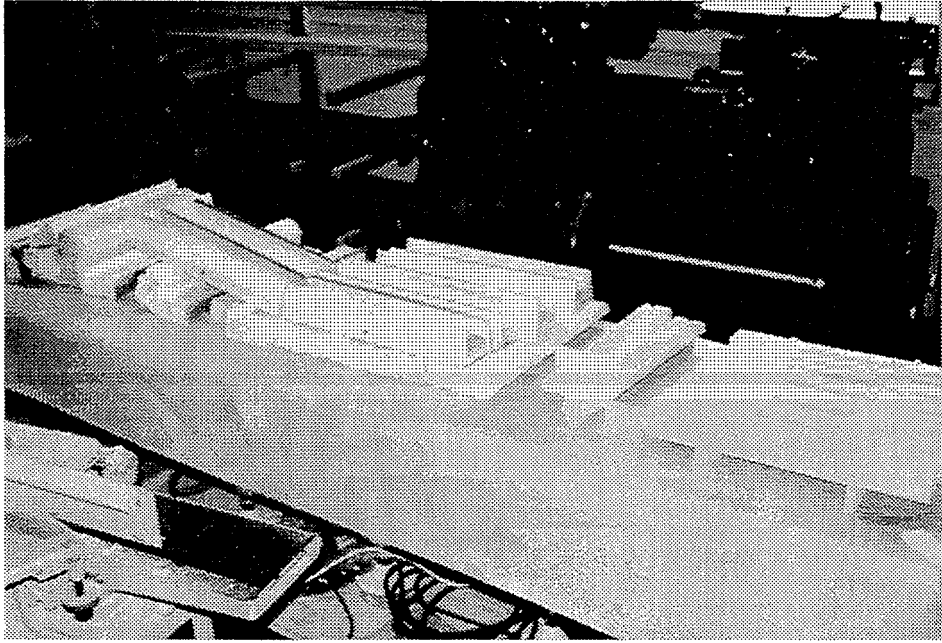


Figure 8. Photographs of blade leading-edge and cove pieces.

Test Turbine

The test site for the NWTC Grumman 20 kW wind turbine is fully instrumented for a comprehensive range of measurements. Minimal modifications were required to accommodate the current tests. The reader is referred to Butterfield (1992) for further information on the turbine, the test site, and the data-acquisition system. Discussions in the following sections will focus on those aspects that are particularly relevant to the investigation.

Blade-root edgewise and flapwise bending moments were measured by a pair of strain-gage bridges mounted at the base of the blades. Position encoders recorded blade pitch angle, as set by the operator, and turbine yaw angle relative to the wind direction. An array of atmospheric sensors measured air pressure and temperature at the site. Five separate anemometers recorded the wind direction and magnitude, as a function of time, height, and lateral position. The rotational speed of the rotor, nominally 72 revolutions per minute (RPM), was also monitored and measured. Data from these particular sensors were used to identify device-related loads and the corresponding aerodynamic coefficients.

The CER turbine includes provisions for the installation of an angle-of-attack measuring "flag" device, but it was not readily moved to different span-wise locations and it was feared that its large size might have an adverse effect on the flow over the test portions of the blade. As a result, the angle of attack was estimated using another process (as will be discussed shortly).

Signals from the various turbine and site sensors were transmitted to the computer-based data acquisition system for real-time display and recording. Calibration data, obtained just prior to tests, were applied so that final measurements were in the appropriate engineering units. The data-acquisition system made approximately 512 measurements per sensor, per second, for a total of 30 rotor revolutions.

Test Configuration

Wind speeds from 1 to 5 meters per second (\approx 2.0 to 8.0 mph) were expected during the scheduled test period (summer) at the NWTC. Sustained and reasonable data-acquisition rates for the turbine in this condition seemed unlikely. As a result, the machine was operated in a "motored" configuration.

Preliminary calculations, using the PROP93 (McCarty 1993) wind turbine performance prediction code (in a motored mode), indicated that it would take too much time for the wake of a three-bladed rotor to convect downstream at the anticipated low wind speeds. Thus, to minimize the possibility of significant wake interactions, a one-bladed rotor with counter weights was used. Operating the machine in a motored and single-bladed configuration offered opportunities for a more controlled test progression. Figures 9 through 12 show diagrams and photographs of the turbine and test blade with aerodynamic controls.

Flow visualization experiments were conducted prior to the primary tests to verify that the blade wake would convect downstream, as desired. The blade tip was fit with a "smoke grenade" and operated over a range of wind speeds, blade pitch settings, and yaw angles. As Figure 13 shows, the tip flow was moved away from the rotor blade, prior to its next sweep, as long as the wind speeds were above approximately 2 meters per second (\approx 4.5 mph). These results agreed well with those from the PROP93 code runs. As the investigation proceeded, every effort was made to take data only when the winds were above this threshold value.

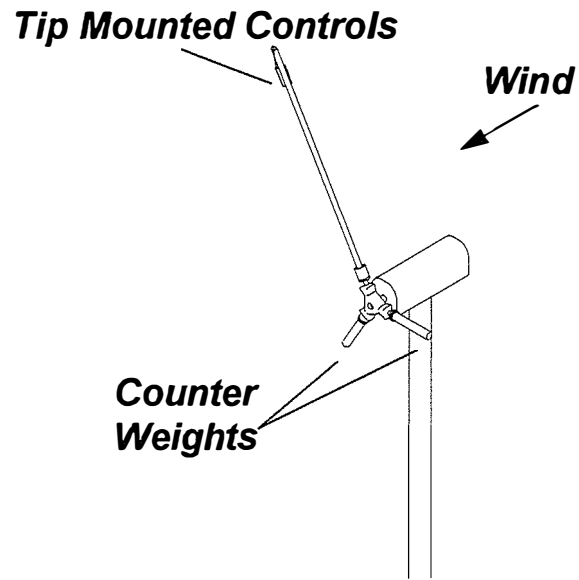


Figure 9. Simple diagram of the single-bladed downwind rotor, as used in the investigation.

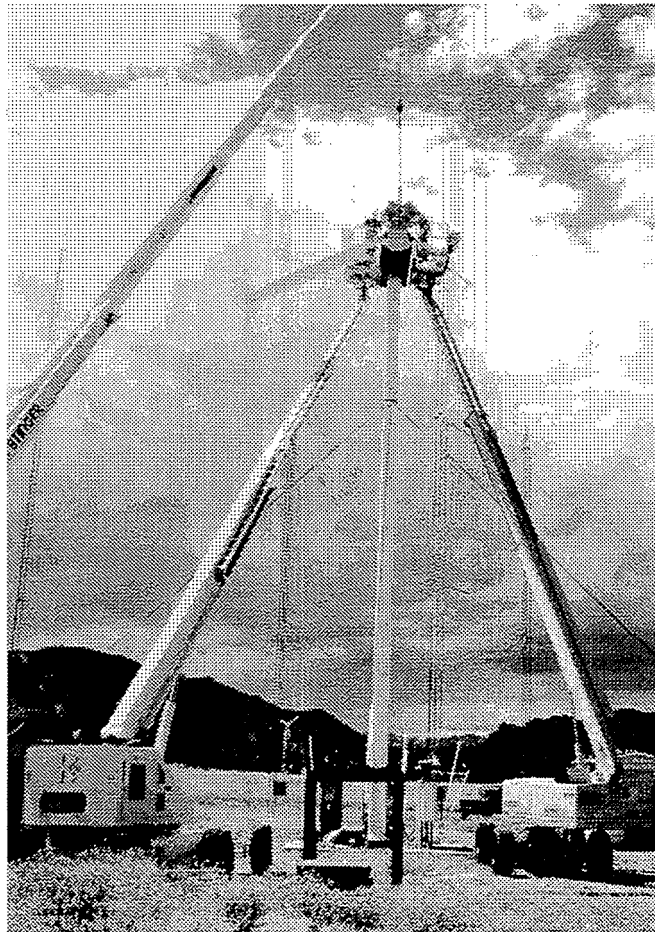


Figure 10. Installation of test blade and counter weights on the "CER" turbine.

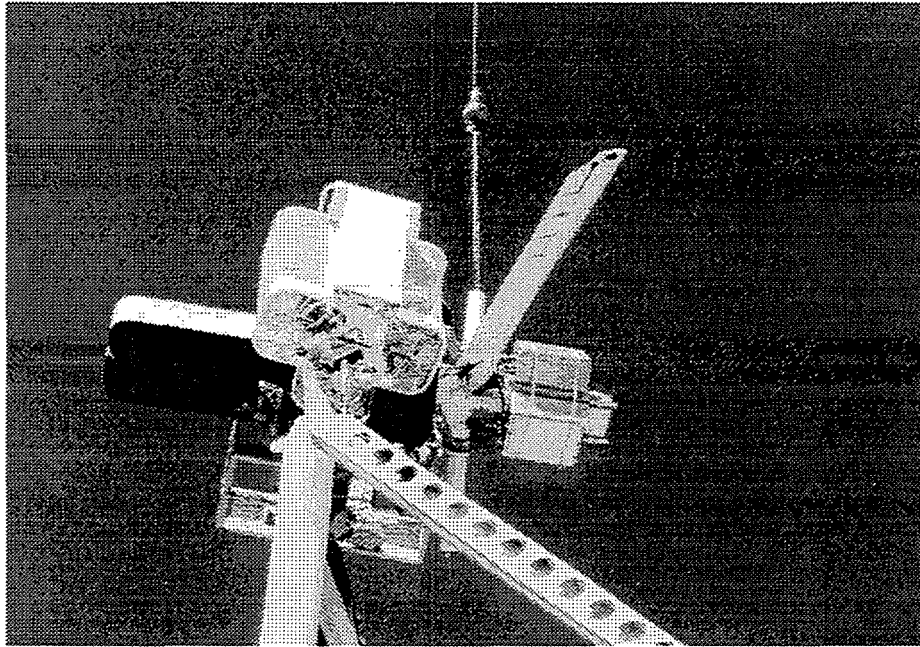


Figure 11. Counter weight installation on the "CER" turbine.

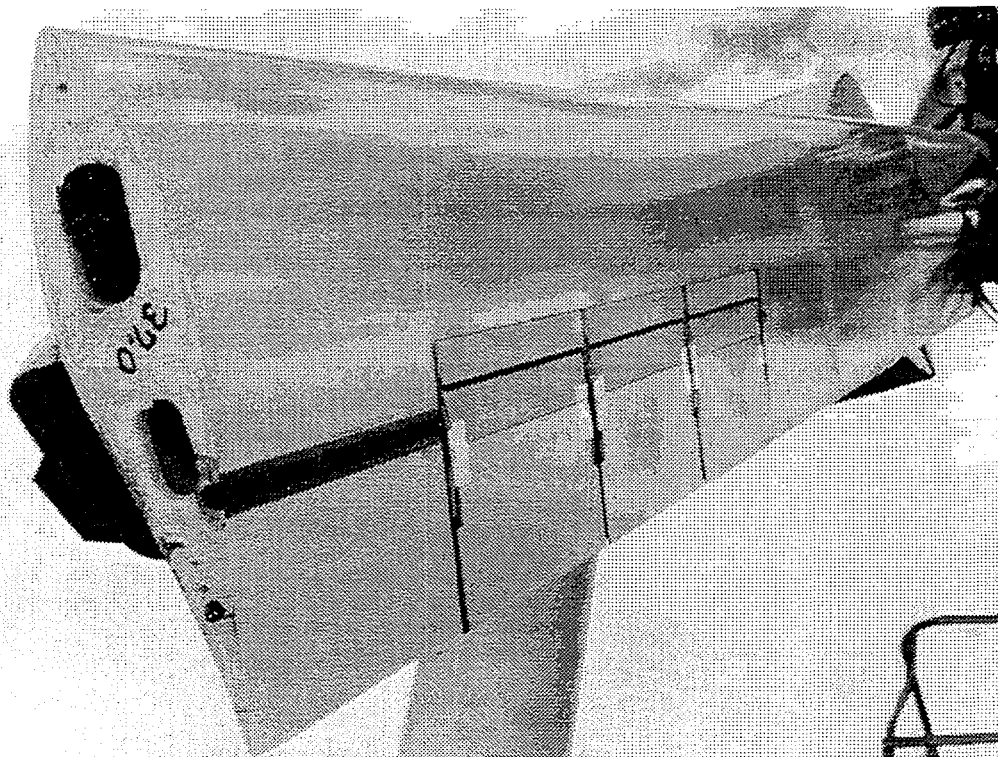


Figure 12. Close-up of test blade (without tip cover) and aerodynamic control devices in undeployed positions.



Figure 13. A photograph from the flow visualization investigation.

Test Procedure

Along with the flow visualization experiments, a significant amount of time was expended calibrating the various sensors on the turbine and the blades. Most important were the blade-root moment strain gages and the device hinge-moment apparatus. Each of these components was sequentially loaded, in both positive and negative directions, through its maximum expected range. The calibrations were performed with the blades mounted to the turbine.

Once the necessary calibrations were completed, the primary investigation began. Table 1 identifies the test configurations that were examined for each device and gives a basic idea of how the tests were conducted. In summary, a particular device configuration was set up, the motor was turned on, the blade pitch was swept through the desired range, and the data were recorded.

The type of device (i.e., spoiler-flap, vented aileron, or unvented aileron), the deflection angle, and the span were set manually prior to running. The data acquisition system was triggered after the rotor speed stabilized and the blade pitch was adjusted to the desired value. A "manually actuated" yaw-brake was used in an attempt to minimize turbine pointing error, but unfortunately the wind direction varied rapidly during some of the runs. As will be discussed later, the data were filtered during analysis to use only the measurements that fell within a specified threshold of yaw.

Table 1. Device configuration and condition test summary.

Device Deflection Angle:	$\delta = 0, 10, 30, 60, 90$ degrees
Blade Pitch Angle:	$\beta = 0, 5, 9, 12, 15, 18, 21, 26, 31, 36, 41$ degrees
Device Span:	$\Delta r = 7.5\%, 15\%, 22.5\%$

Test Reynolds Numbers

Table 2 shows approximate Reynolds numbers (based on a blade chord of 0.46 m) at the mid-span of each device, assuming a fixed rotor rotational speed of 72 rpm and a wind speed of between 2 and 5 m/s. As is shown, the Reynolds number was essentially 1,000,000 for typical operating conditions and all three device spans.

Table 2. Mid-span Reynolds numbers, for each device span.

<u>7.5%-Span Device</u>	<u>15%-Span Device</u>	<u>22.5%-Span Device</u>
$Rc \cong 1,035,000$	$Rc \cong 990,000$	$Rc \cong 951,000$

Data Reduction

Almost two gigabytes of binary-format data were collected during the eight-week investigation. A primary goal was to convert this information into a form similar to that obtained from the wind tunnel tests. Plots were calculated showing the aerodynamic lift, drag, suction, and hinge-moment coefficients as a function of angle of attack, deflection angle, and span. A great deal of time and effort was required to complete this part of the project.

As was expected, measurements made during the tests were unsteady. The combined effects of inflow variations, gravity, and blade dynamic responses, for example, resulted in a notable change in the root-bending moments as a function of time. Because of these effects, all measurements were averaged over individual rotor rotations, or cycles, for a total of approximately 30 revolutions. To assure quality results, data with yaw errors greater than fifteen degrees were excluded during this averaging process.

Aerodynamic Coefficients

Because the blade-root strain-gages measured the behavior of the entire blade, not just that of the aerodynamic device, it is not possible to calculate absolute device aerodynamic coefficients (i.e., C_l , C_d , and C_s). However, a measure of the device's effect can be identified by simply taking the difference between deflected and nondeflected root-bending moments. It is assumed that the observed changes in root moments are a direct result of the device configuration and deflection.

It is important to note, within the above mentioned assumption, that aerodynamic changes are exclusively attributed to the effect of the device and that flow behavior changes over the rest of the blade are neglected. Unfortunately, turbine measurement provisions and analysis limitations prevented a more detailed accounting of the entire blade's aerodynamic character.

Changes in the aerodynamic behavior of the control devices are described using "delta-coefficients" (i.e., ΔC_n , ΔC_s , ΔC_l , and ΔC_d). The formulas defining the C_n and C_s delta-coefficients are as follows.

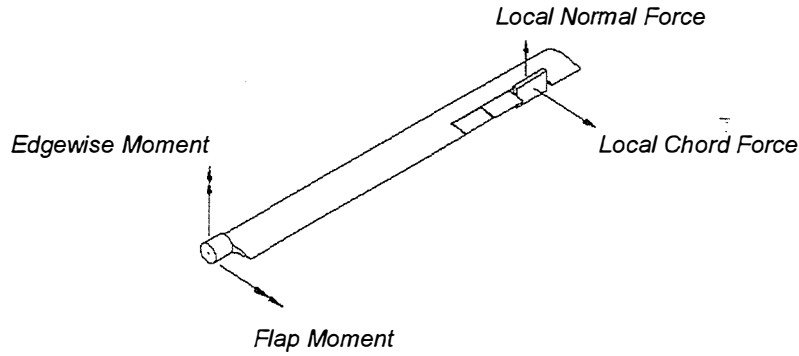
$$\Delta C_n = [M_{F\delta}/q_\delta - M_{Fo}/q_o] [1/(Sr)]$$

$$\Delta C_s = [M_{E\delta}/q_\delta - M_{Eo}/q_o] [1/(Sr)]$$

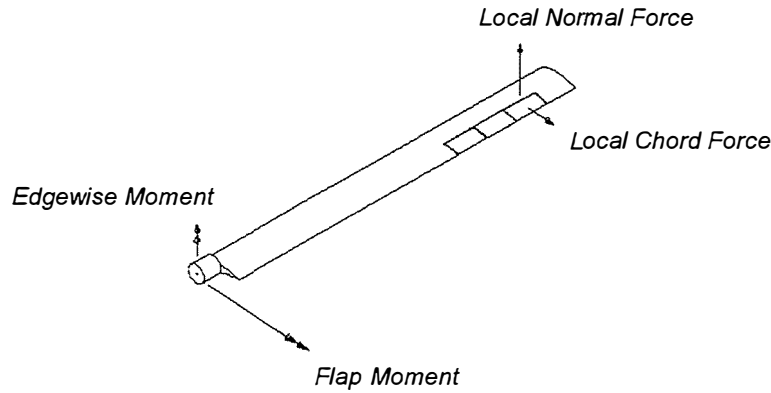
M_F and M_E are, respectively, the blade-root flap and edgewise moments at a dynamic pressure "q." The subscript "δ" indicates a deflected (i.e., $\delta \neq 0$) control device and the subscript "o" represents a "baseline" undeflected (i.e., $\delta = 0$) case. "S" is the blade area over which the device is active and "r" is the radial distance to the device centerline. " ΔC_n " represents the change in the aerodynamic normal-force (i.e., in a direction perpendicular to the device chord line) and is, hence, directly related to the blade-flap moment. " ΔC_s " represents the change in the suction coefficient and thus directly influences the blade edgewise moment.

The undeflected ($\delta = 0$) spoiler-flap configuration was used as the baseline case from which all delta-coefficients were calculated. The spoiler-flap was selected as the baseline because it most resembled an unmodified blade, in that it had the least aerodynamic-shape deviation from an S809 airfoil. The vented and unvented ailerons have more surface-geometry differences than the spoiler-flap.

Figure 14 illustrates the ΔC_n and ΔC_s concept used to identify the effect of each device on the blade's aerodynamic performance. The delta-coefficient values are obtained by taking the difference between Cases A ($\delta \neq 0$) and B ($\delta = 0$).



Case A – Aerodynamic device defl with reduced normal and increased chord-force components.



Case B – Aerodynamic device undeflected (baseline case).

Figure 14. Diagrams showing changes in blade-root moments, as a result of device deflection (i.e., Case A) relative to zero deflection (i.e., Case B).

These delta-force coefficients can be used to calculate the familiar lift and drag coefficient values by applying the following transformation equations.

$$\begin{aligned}\Delta C_l &= \Delta C_n \cos \alpha + \Delta C_s \sin \alpha \\ \Delta C_d &= \Delta C_n \sin \alpha - \Delta C_s \cos \alpha\end{aligned}$$

The dynamic pressure and angle of attack are calculated at the device mid-span, as follows.

$$\begin{aligned}q &= 1/2 \rho [V_{wind}^2 + (\Omega r)^2] \\ \alpha &\cong \tan^{-1} [\Omega r / V_{wind}] + \beta\end{aligned}$$

The density (ρ) is calculated based on the average air temperature and pressure and " V_{wind} " is calculated as the time average of the site anemometer readings. Device angle of attack (α) is approximated by resolving the device mid-span rotational velocity vector (Ωr), the average wind speed (V_{wind}), and the blade pitch angle (β) into the appropriate directions. The above equations obviously ignore the induced velocity components, produced as a result of the blade's "action" on the flow. Unfortunately, the induced velocity could not be measured, or even estimated, during the tests.

Blade-root-moment plots, normalized by the corresponding dynamic pressure, were obtained for each test condition (i.e., blade rotation, device configuration, and deflection angle (δ)) as a function of angle of attack. To facilitate calculations over a more continuous angle of attack range (i.e., at different-than-

measured angles of attack), the normalized moment results were curve-fit using fourth-order polynomial functions. Figure 15 shows an example of some data obtained and the resulting curve fits. Each symbol represents the calculated cycle average. Groupings of symbols represent data obtained for the total time of testing at a given blade pitch angle, for less than 15 degrees rotor yaw. The scattering of data point groups illustrates the unsteady nature of atmospheric and full-scale testing. The impact of these unsteady effects on the calculated device aerodynamic performance is addressed in the section on Uncertainty Analysis.

Once all of the data were curve-fit, delta-coefficient values were calculated relative to the zero-deflection condition at even intervals over the angle of attack range.

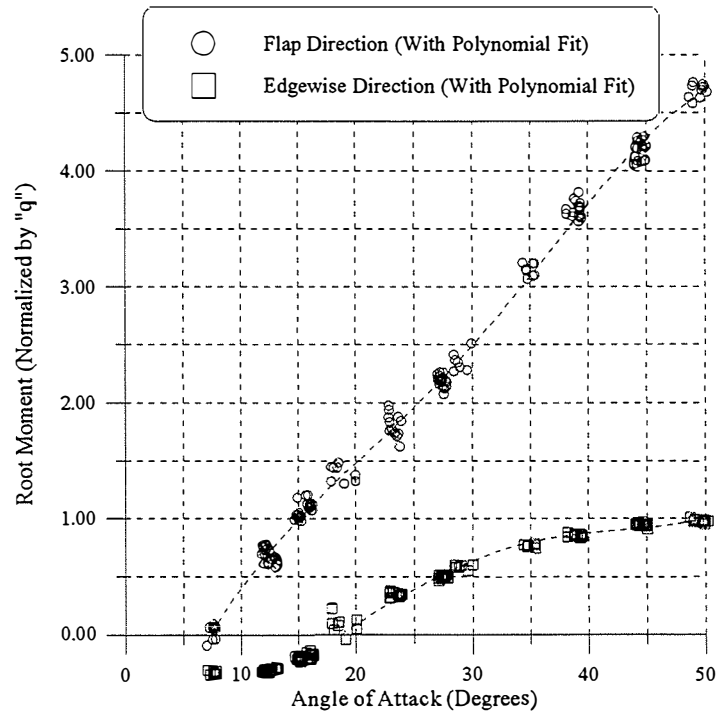


Figure 15. Sample data showing the cycle-averaged data and the variation of normalized blade-root moments with angle of attack.

Hinge-moments

Hinge-moments were calculated using measurements and the equation shown below. In all cases, the sign convention assumes that a positive hinge-moment tends to move the device trailing-edge downward.

$$Cm_h = M_h / (qSc_c)$$

" M_h " is the aerodynamic moment applied to the device, " q " is the mid-span dynamic pressure, " S " is the blade area over which the device is active, and " c_c " is the device chord.

Presentation of Force-Coefficient Results

Aerodynamic-force coefficient results are presented in plots on the following pages. Of prime interest is the finite-span (i.e., three-dimensional) aerodynamic behavior compared to the infinite-span (i.e., two-dimensional) wind tunnel tests. Recall that the suction-coefficient and in particular a reduction in C_s is a measure of the device's ability to influence rotor torque and, as a result, is of prime interest. Because of their common usage, plots showing the lift and drag variations are also included. The data are presented as a change relative to a baseline configuration (i.e., relative to the undeflected spoiler-flap). The infinite-span wind tunnel data were obtained from (Ramsay, Janiszewska, and Gregorek 1996).

Because this report attempts to document all investigation results, a great deal of data are presented in the following subsections. The reader may wish to focus more of their attention on the "Discussion of Force-Coefficient Results" section. That section addresses the perceived significant or key results as most related to the finite-span versus the infinite-span effects.

Spoiler-Flap

Figure 16 shows the spoiler-flap's delta-suction coefficient (ΔC_s) variation for several device deflections as a function of angle of attack. For good turbine braking, a large negative change in the ΔC_s value is desirable.

For angles of attack less than stall (approximately 17 degrees) and device deflections below 60 degrees, a clear relationship between the infinite and finite-span results is difficult to identify. However, when the device deflection is 90 degrees, the wind tunnel data clearly predict a much larger drop in suction-coefficient than any of the partial-span configurations. As one might expect; a large-span device is more effective, but still not equal to a two-dimensional case.

For angles of attack greater than stall and all device deflections, the 15% and 22.5%-span devices appear approximately equal in ΔC_s capability. This observation suggests that span effects are more pronounced for shorter span devices. Unfortunately, infinite-span data were not available for angles of attack greater than about 27 degrees and comparisons could not be made between wind tunnel and field-test results.

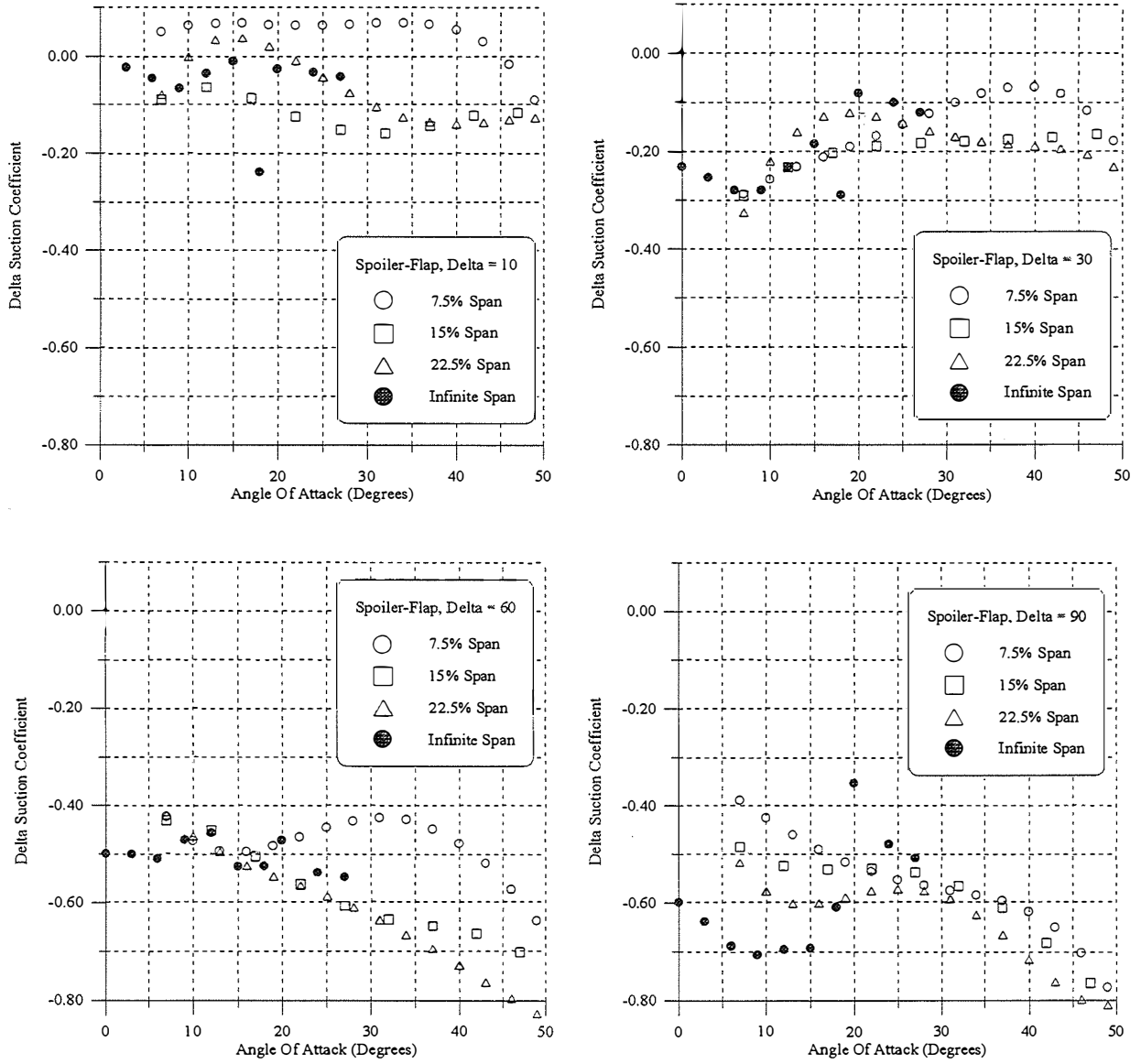


Figure 16. Spoiler-flap delta-suction coefficient for various spans.

Figure 17 shows the spoiler-flap's delta-lift coefficient (ΔC_l) variation for various device deflections and angles of attack. For good turbine braking, a large negative change in ΔC_l is desirable.

The infinite-span data show that stall occurs at an angle of attack of approximately 17 degrees, as evidenced by a sudden discontinuity in the ΔC_l variation. The finite-span cases do not exhibit the same discontinuity.

For all cases except a device deflection of 10 degrees, the infinite-span wind tunnel test results under-predict the lift loss. Interestingly, the shorter (i.e., 7.5%) span device appears to generate a greater reduction in lift-coefficient. Except for $\delta = 10$ degrees and around stall, the 22.5%-span device generates ΔC_l values similar in magnitude to the wind tunnel results.

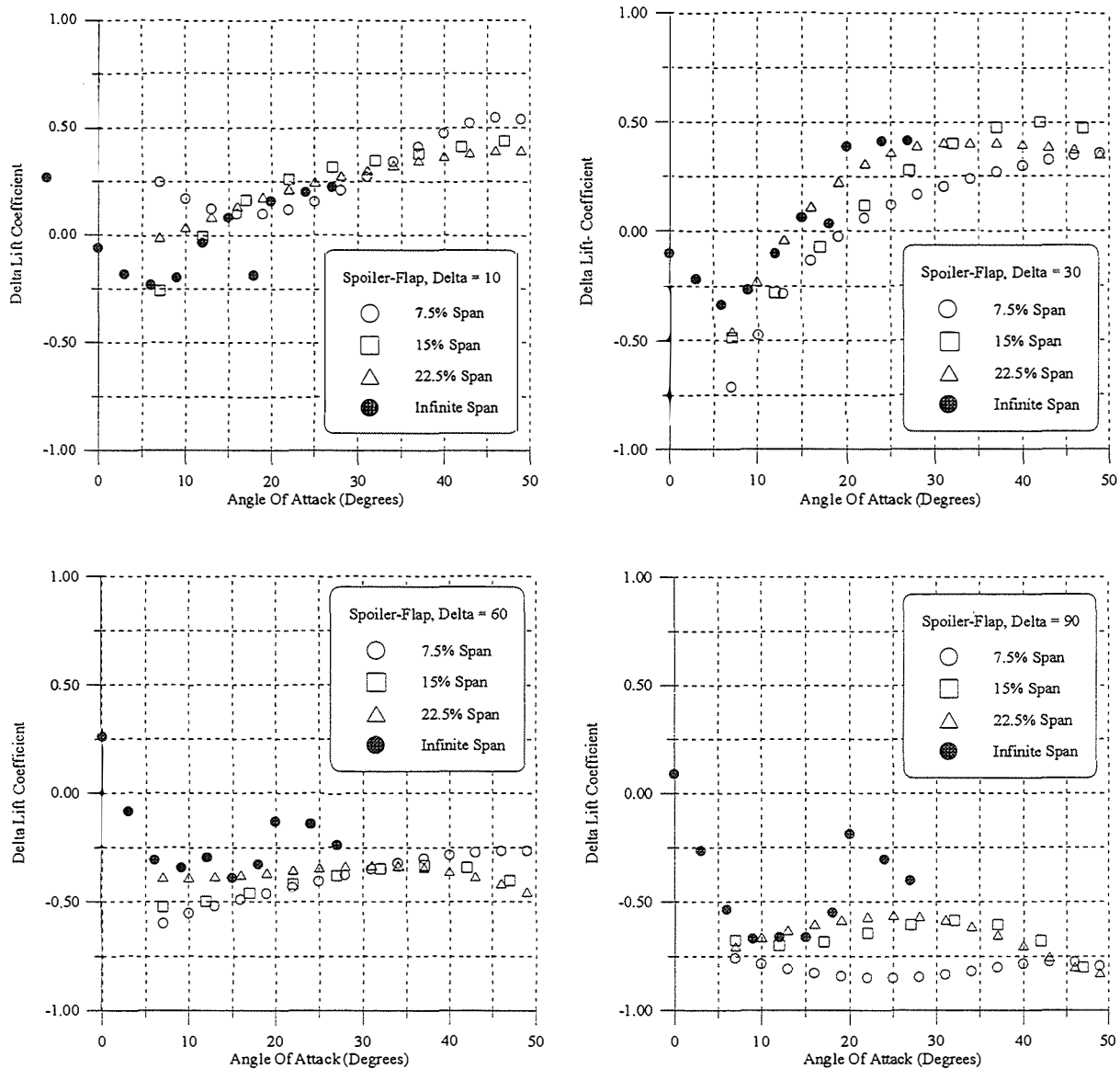


Figure 17. Spoiler-flap delta-lift-coefficient for various spans.

Figure 18 shows the spoiler-flap's variation of delta-drag-coefficient (ΔC_d). For good turbine braking capability, a large positive change in ΔC_d is desirable. As was the situation in some previous cases, for device deflections of 30 degrees or larger, the infinite-span data predict a slightly greater increase in drag than is observed for a finite-span configuration. Again the 15% and 22.5%-span devices generate similar changes in the drag (better than those of the shorter 7.5%-span) for angles of attack above approximately 17 degrees.

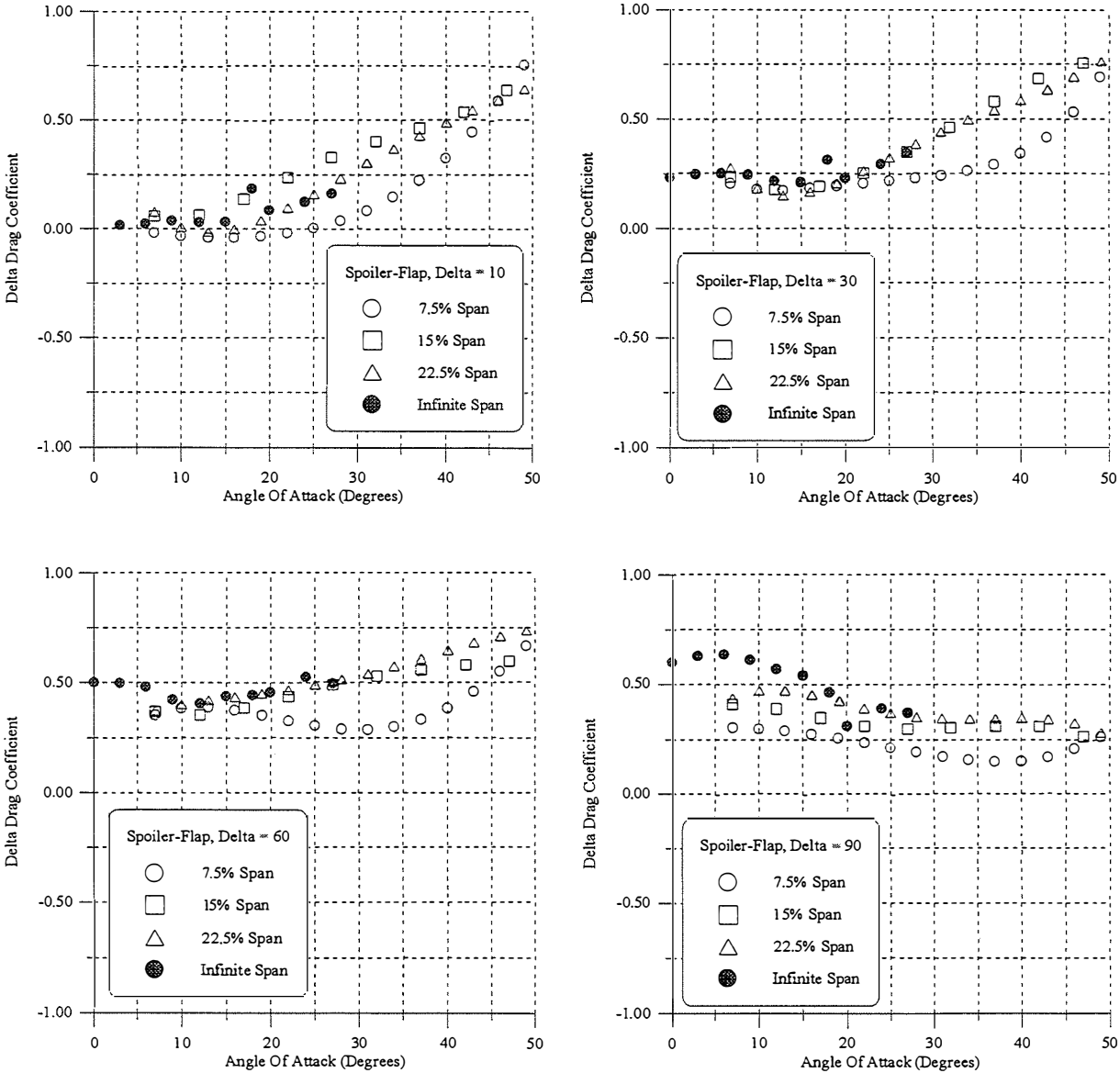


Figure 18. Spoiler-flap delta-drag coefficient for various spans.

Vented Aileron

Results for this configuration are similar in many ways to those of the spoiler-flap. Figure 19 shows the ΔC_s data for the vented aileron configuration. For angles of attack below approximately 17 degrees, the finite-span results are of lower magnitude (i.e., not as negative as is desired) when compared to the two-dimensional data. However, at higher angles of attack and device deflections (i.e., $\delta > 60$ degrees) the reduction in finite-span suction coefficients is greater than that for the wind tunnel data. As was noted previously, the larger 15% and 22.5%-span devices perform similarly, typically better than the shortest-span device.

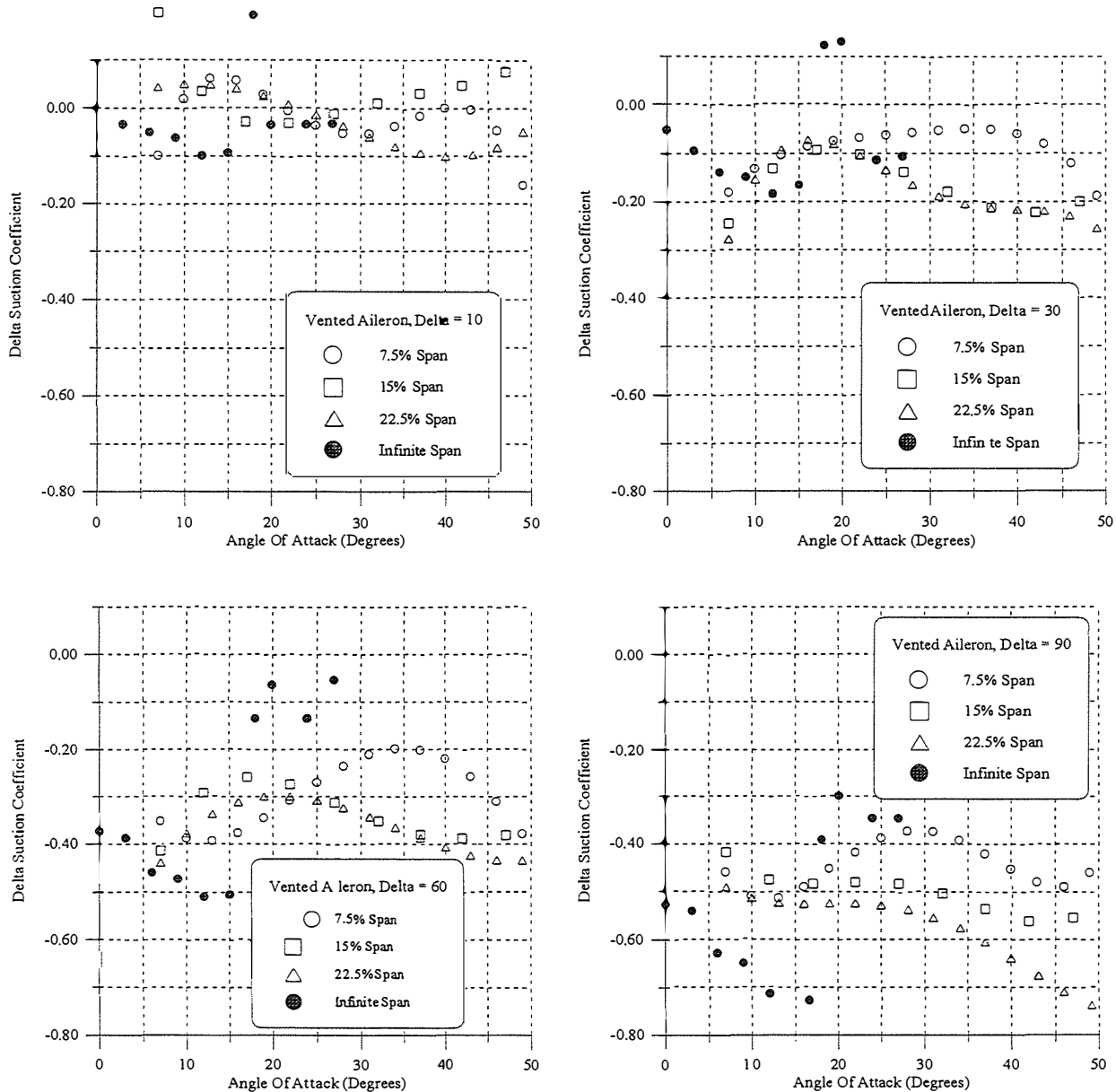


Figure 19. Vented aileron delta-suction coefficient for various spans.

Figure 20 shows the vented aileron's delta-lift coefficient (ΔC_l) behavior. In contrast to the spoiler-flap, the finite-span vented aileron configuration differed less in behavior relative to the infinite-span case. The finite-span stall behavior is again softened, relative to that observed for the wind tunnel configuration. The greatest differences in ΔC_l behavior are noted for the shortest (i.e., 7.5%) span and at angles of attack around 17 degrees, and for device deflections of 30 and 90 degrees.

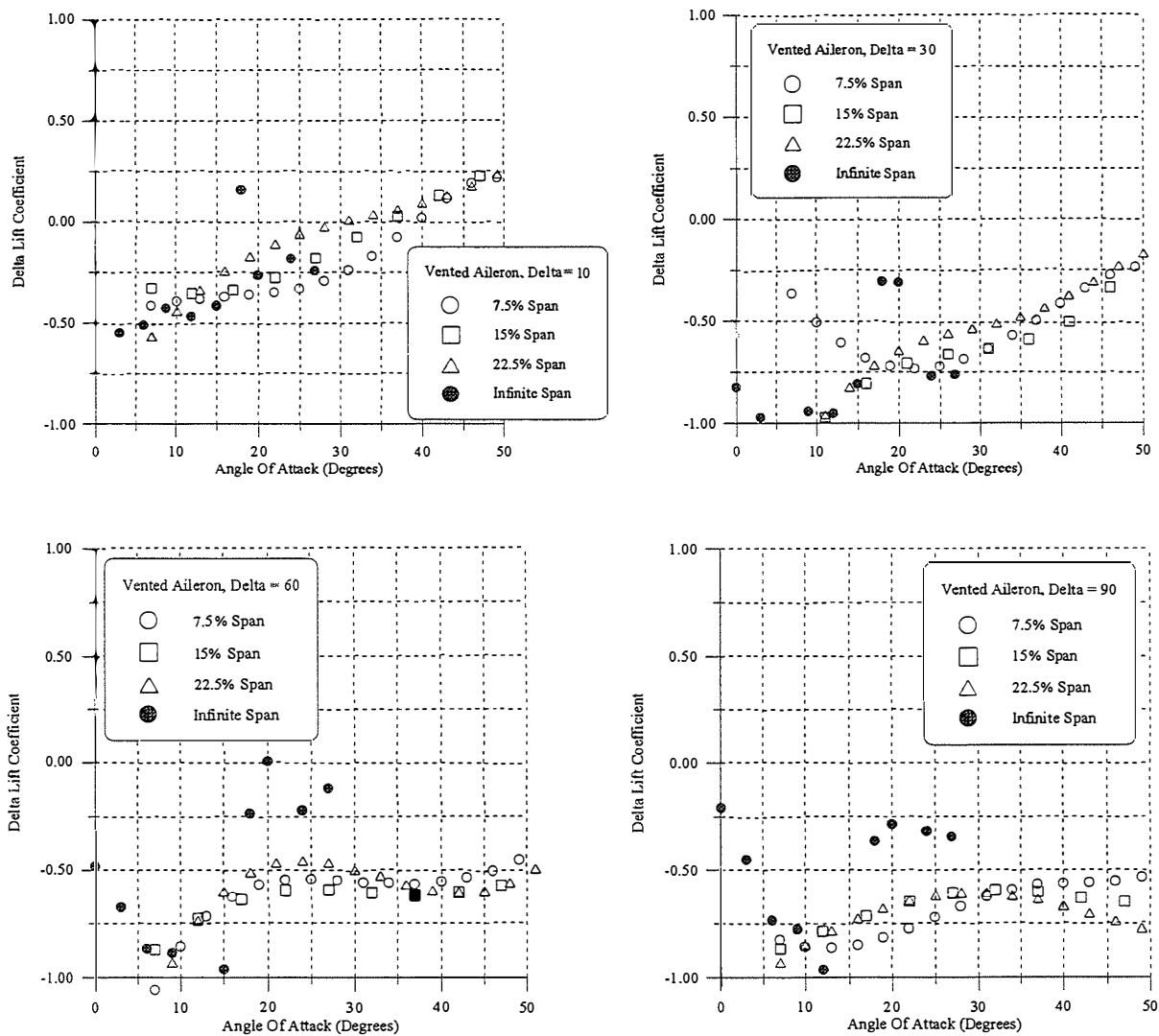


Figure 20. Vented aileron delta-lift coefficient for various spans.

Figure 21 shows the vented aileron's delta-drag coefficient (ΔC_d) behavior. For angles of attack below about 17 degrees the change in drag for the infinite-span configuration appears similar or slightly lower than is observed for finite-spans. Interestingly, at higher angles of attack (i.e., $\alpha > 20$ degrees) the shorter-span device offers the better (i.e., higher) drag performance.

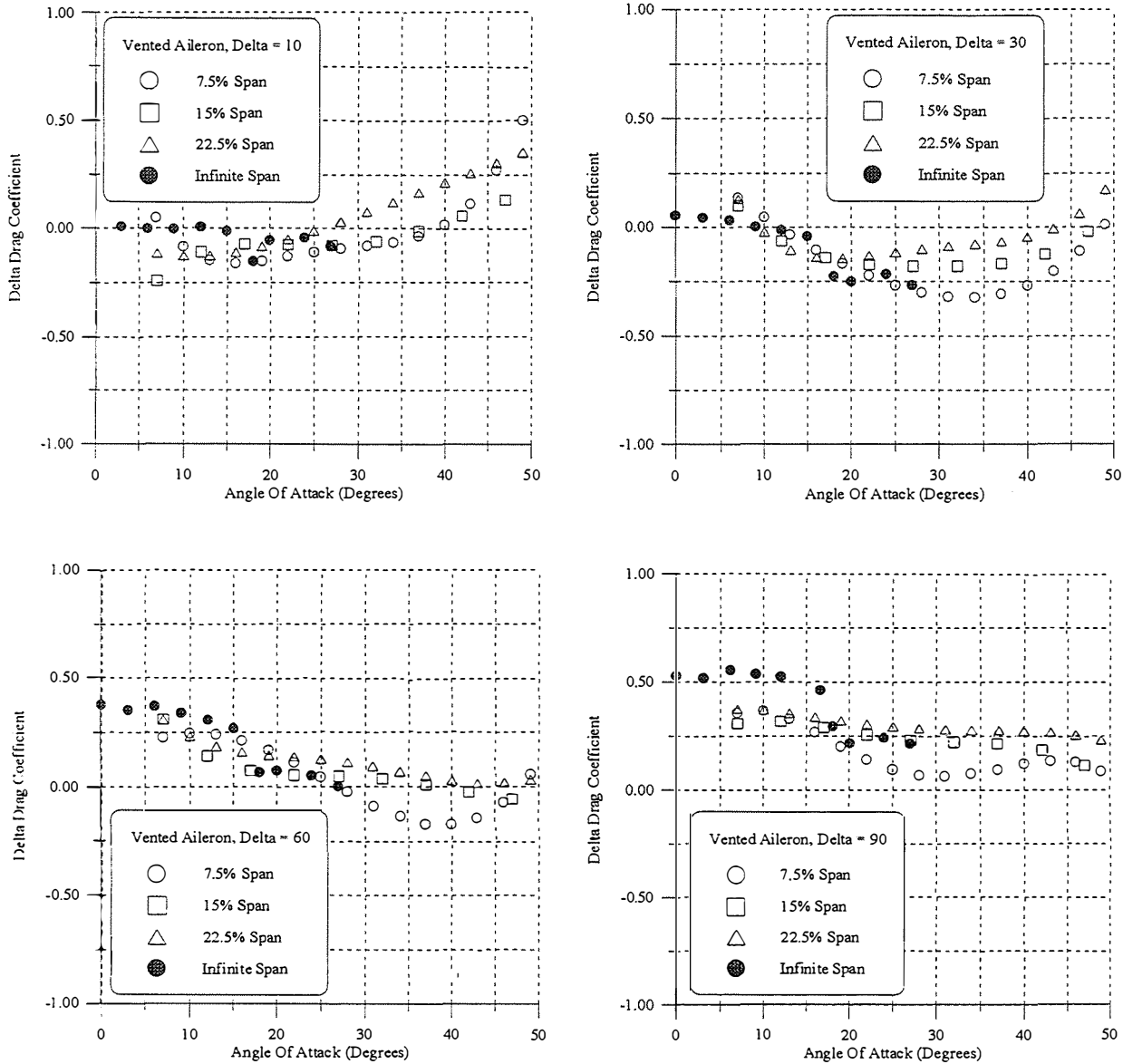


Figure 21. Vented aileron delta-drag coefficient for various spans.

Unvented Aileron

Figure 22 shows the unvented aileron's variation of delta-suction coefficient (ΔC_s) for various device deflections and angles of attack. Unfortunately, it was discovered after the atmospheric tests were completed that the data for the 22.5%-span configuration were corrupted for all device deflections (i.e., δ 's) other than 90 degrees.

The differences between the wind tunnel and finite-span configurations are difficult to identify. For a device deflection of 60 degrees, the infinite-span suction-coefficient reduction is lower than that observed for the finite-spans at angles of attack below approximately 15 degrees. As has been the case for the other aerodynamic device configurations, a span greater than 7.5% appears desirable.

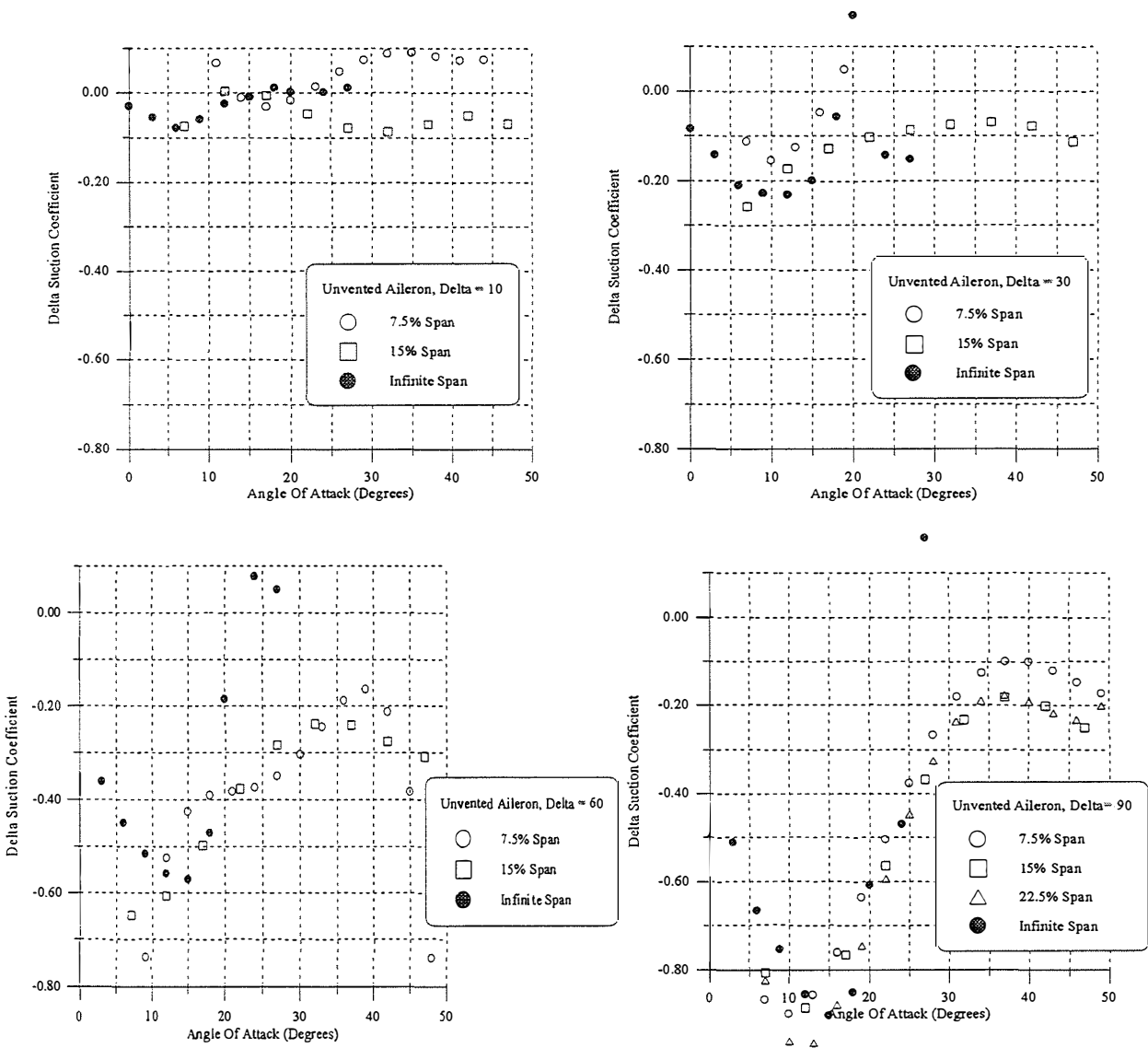


Figure 22. Unvented aileron delta-suction coefficient for various spans.

Figure 23 shows the unvented aileron delta-lift coefficient (ΔC_l) behavior. Note that the ordinate of each of these plots has been shifted to show more negative values. Other plots in this section of the report show ΔC_l values ranging from -1.0 to +1.0, Figure 23 shows ΔC_l values from -2 to 0.0. This deviation was necessary because the negative camber of the unvented aileron configuration produces extremely large reductions in lift. For angles of attack less than about 15 degrees, the infinite- and finite-span data are very similar. Interestingly, for angles of attack above 15 degrees and device deflections greater than 60 degrees, the shorter span device generated the larger reduction in lift coefficient.

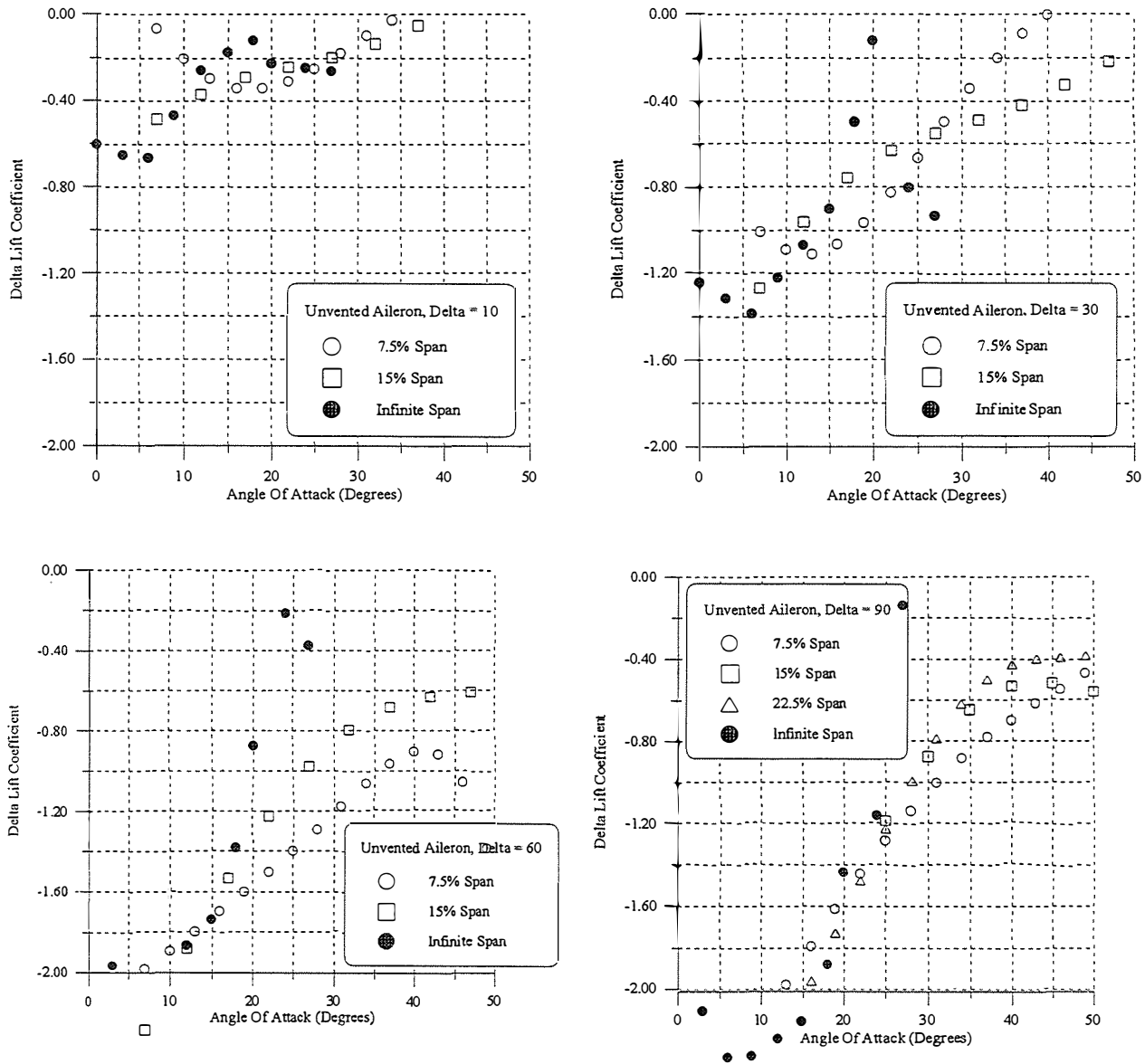


Figure 23. Unvented aileron delta-lift coefficient for various spans.

Figure 24 identifies the unvented aileron delta-drag coefficient (ΔC_D) behavior. As was the case for lift, the drag coefficient effects are very similar, regardless of span, at angles of attack below approximately 15 degrees. At higher angles of attack the larger span (i.e., >15%) devices offer a greater increase in drag coefficient.

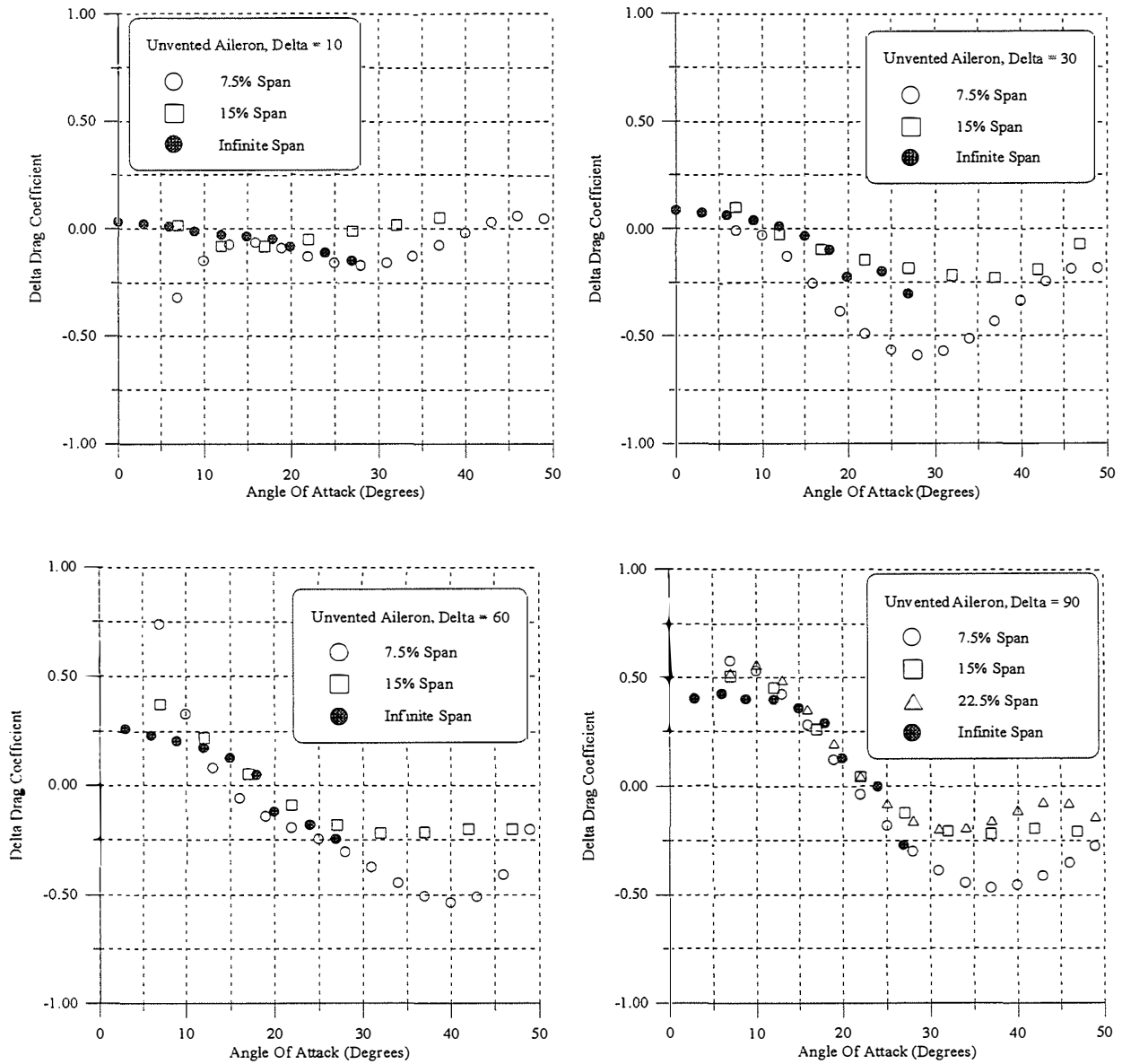


Figure 24. Unvented aileron delta-drag coefficient for various spans.

Discussion of Force-Coefficient Results

As is no doubt obvious, a great deal of data has been presented in the previous section. This part of the report provides an overview of the perceived most important and significant results as related most to the investigation objectives.

It is important to identify, if possible, a means for estimating the change in device performance from infinite-span to finite-span cases. Consequently, some observations of span effects, on the lift and drag behavior, are offered. The ideas and comments apply in a general sense to each of the three configurations examined and especially to the spoiler-flap and vented aileron.

Span Effects and Lift

As has been shown, a reduction in device span results in a "softening" of the stall behavior. Changes in the ΔC_l curves, around stall or approximately 17 degrees angle of attack, are less abrupt when compared to the variations observed for the infinite-span devices. Such effects are to be expected, as a result of aspect ratio reductions, and are observed for other similar geometry's like wings and flat plates.

The largest span device (i.e., 22.5%) produced ΔC_l values that are similar in magnitude to the infinite-span. Curiously, the shortest span device (i.e., 7.5%) appears to produce the largest reduction in lift coefficient. This result seems unreasonable and suggests that some other phenomena may be contributing to the observed results. Perhaps the unmodified inboard part of the blade is being affected notably as a result of the device deflection. As Figure 25 shows, by unloading the device portion of the blade a strong shed vortex could be forming at an effectively new blade tip, so as to induce a notable reduction in the angle of attack on the inboard working part of the blade. This angle of attack reduction would in turn cause a drop in the blade flapping load and hence could be wrongly interpreted as a device (alone) effect, when in reality it is also an inboard blade effect. The vortex strength and its influence would diminish as the effective blade tip moved inboard, thus explaining why the ΔC_l magnitude drops as the device span is increased. A great deal of time and effort was expended to verify this hypotheses and to analytically quantify the effect. Unfortunately, a simple correction scheme was not identified. Work will continue in this area.

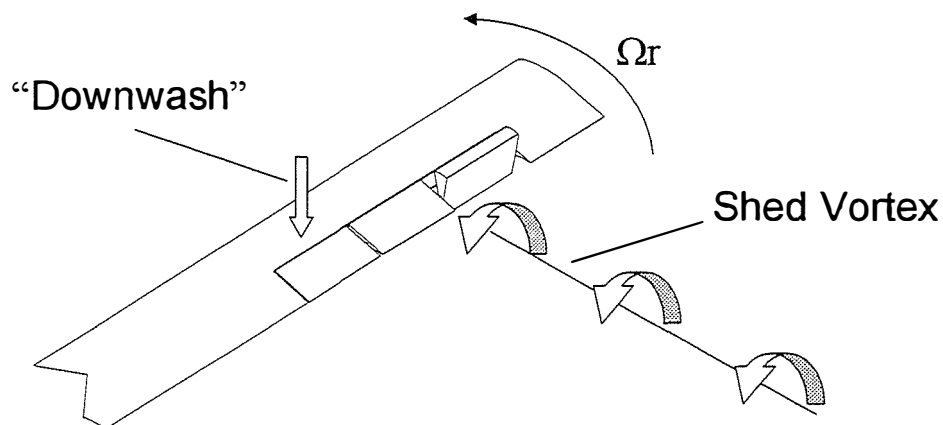


Figure 25. Diagram illustrating the inboard angle of attack reduction or downwash induced by a shed vortex.

Span Effects and Drag

As was noted in much of the data presented earlier, the shortest (i.e., 7.5%) span configuration typically produced the smallest drag change (i.e., ΔC_d) and, as might be expected, the infinite-span device produced the greatest change in drag. Most significantly, the 15% and 22.5%-span devices behaved similarly and were closer, yet smaller in magnitude, to the infinite-span case. This particular behavior is consistent with that observed for other two- and three-dimensional shapes.

As was shown by Hoerner (1958) for simple geometries with height-to-span ratios below approximately 0.20, the drag coefficient changes rapidly. At height-to-span ratios above 0.20 the drag behavior is nearly constant and roughly 60% of the infinite-span value. Figure 26 illustrates this effect, for a rectangular plate and a circular cylinder. Hoerner further suggested the following approximate expression for the observed effects (Hoerner 1958, Equation 29, p. 3-15):

$$\lambda \equiv [(C_d)_{3D}/(C_d)_{2D}] \cong 1 - K(h/b)$$

Where λ is the ratio between the finite and infinite-span drag coefficients, h is the height, b is the span, and K is a constant of order 5.0

The above equation can be modified to fit the current applications, as follows.

$$\lambda_d \equiv [(\Delta C_d)_{3D}/(\Delta C_d)_{2D}] \cong 1 - K'(c_c/\Delta r)$$

Where λ_d is now the ratio between the finite and infinite-span delta-drag coefficients, c_c is the device chord, Δr is the device span, and K' is again a constant. On the basis of a limited amount of data, for the configurations examined in this investigation, a value of K' equal to approximately 1.1 appears to best fit the results.

Figure 27 compares the results predicted for a 7.5%-span spoiler-flap ($c_c/\Delta r = 0.485$ and $\lambda_d = 0.47$), as obtained by applying the above expression to the infinite-span data. The results are encouraging, with only notable differences at stall-condition angles of attack. λ_d values for 15% and 22.5%-span devices are calculated as, respectively, 0.73 and 0.82

Regardless of the proposed equation's accuracy, the basic trends noted by Hoerner appear to apply to the current investigation's drag results. Formulating an exact equation is difficult. The shapes of interest (i.e., the aerodynamic controls) are more complicated than rectangular plates or circular cylinders. In addition, the control surface is typically positioned downstream of an upstream element and there are associated wake-interaction effects.

Given a trailing-edge device geometry (i.e., chord and span), one could use the proposed equation to calculate a λ_d value and then simply multiply it by the infinite-span delta-drag coefficient to identify an approximate finite-span value. Fortunately, the current work suggests that any variances from actual will be on the conservative side.

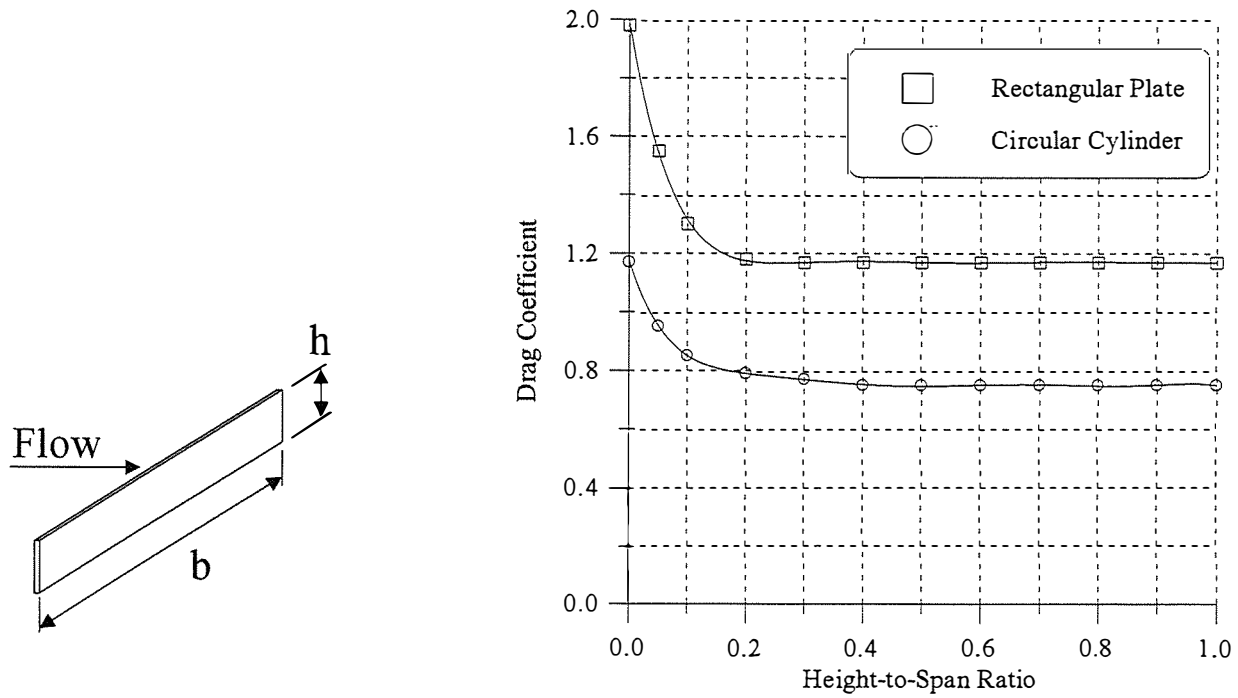


Figure 26. Drag coefficient of two simple shapes, installed perpendicular to the flow, as a function of height-to-span ratio (Hoerner 1958).

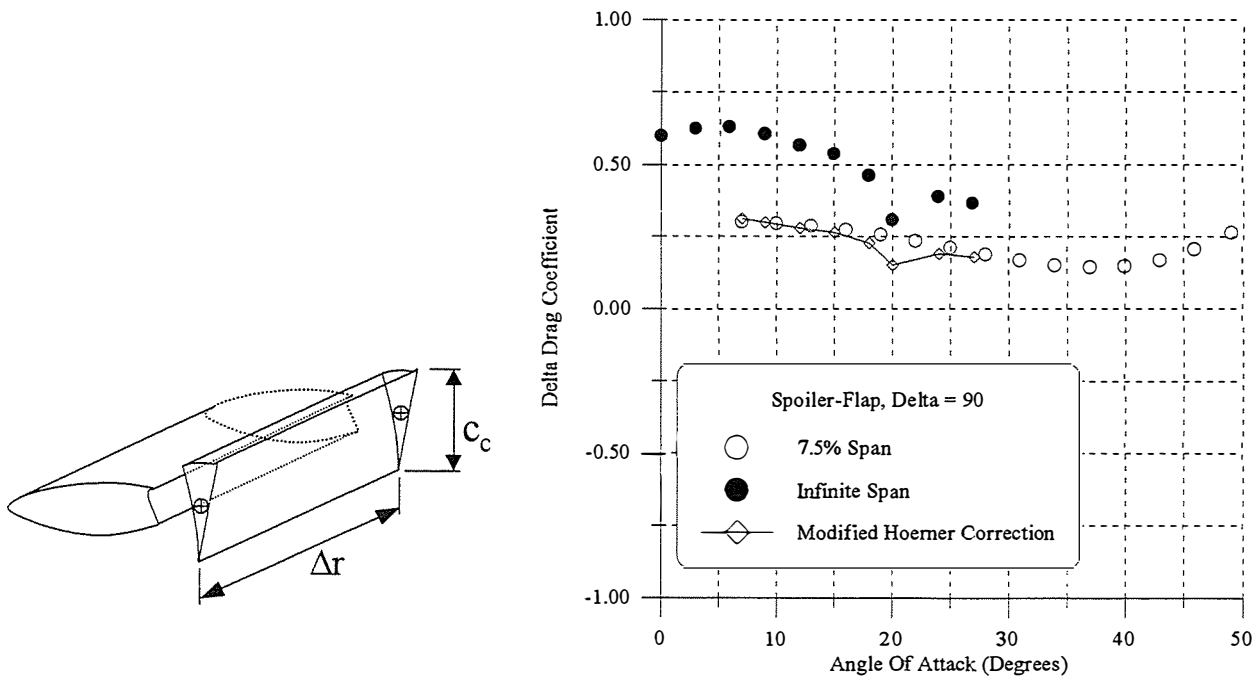


Figure 27. Example of delta-drag coefficient correction, for 7.5%-span spoiler-flap, using modified equation.

Uncertainty Analysis

Measurements gathered during the atmospheric experiments were unsteady as a result of a combination of factors, most notably wind variations and the dynamic response of the blades; the data were cycle-averaged in an attempt to minimize these effects. Nonetheless, the cycle-average values show small, yet notable, variations in both the angle of attack and moment magnitudes for a fixed-blade pitch setting. This result is illustrated in a sample plot presented previously as Figure 15 and again, below, for easy reference. Each symbol represents a cycle-average value and the dashed lines show the curve fits to the data.

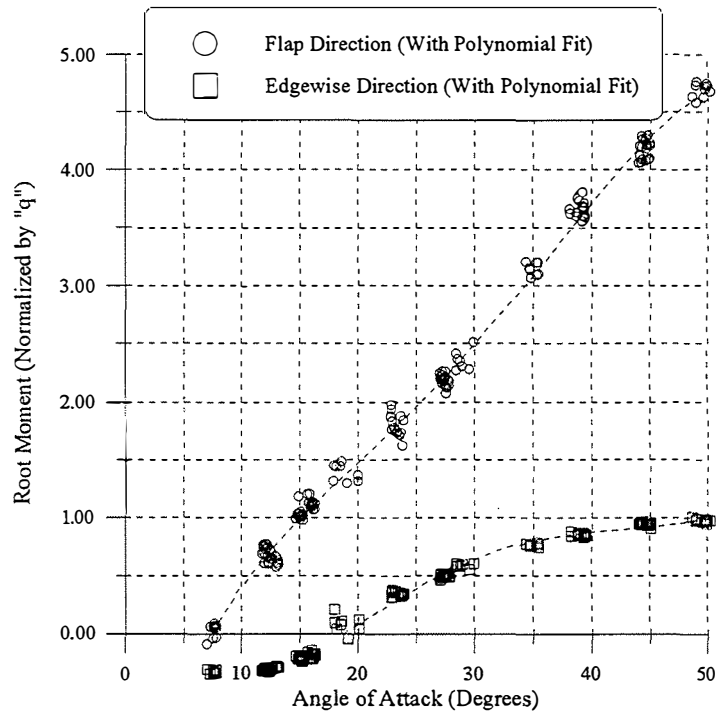


Figure 15 (repeated). Sample data showing the cycle-averaged data and the variation of normalized blade-root moments with angle of attack.

The cycle-averaged root-moment values and curve fits were used to calculate the delta-coefficients for each device. The results of these calculations are presented in previous sections of this report. A measure of the confidence in these results is desirable because of the noted data scatter and the use of a curve fit. Hence the Kline-McCintock uncertainty-analysis method (Holman 1994) was applied to a representative set of spoiler-flap data to evaluate the certainty of the results.

The Kline-McCintock method combines the observed unsteadiness levels and the governing equations to define a standard deviation in the final calculated aerodynamic delta-coefficients. The standard deviation of each parameter was measured during the experiment and utilized in the uncertainty analysis, along with the equations shown in the Aerodynamic Coefficients section of this report. The resulting delta-lift and delta-drag coefficient standard-deviation magnitudes give a statistical measure of the certainty as influenced by unsteady effects.

Figures 28 and 29 show the results of the uncertainty-analysis. The calculated uncertainties (i.e., standard-deviation) values ignore the measurement accuracy of the various CER turbine sensors used in the experiment. This assumption appears reasonable because the observed unsteady variations are significantly larger than the noted CER instrumentation inaccuracies (Butterfield 1992).

The standard deviations in the ΔC_l and ΔC_d values are approximately 0.12 over the entire angle of attack range, with the largest value noted for a 90-degree device deflection. These results suggest that there is roughly a 67% probability that the actual value of the delta-coefficients lies within ± 0.12 of the values shown in the Results section plots.

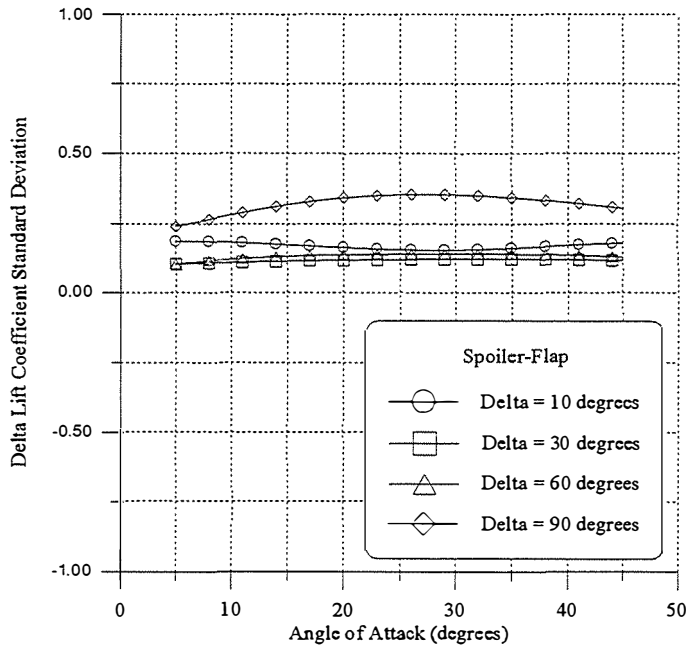


Figure 28. Spoiler-flap ΔC_l uncertainty analysis results.

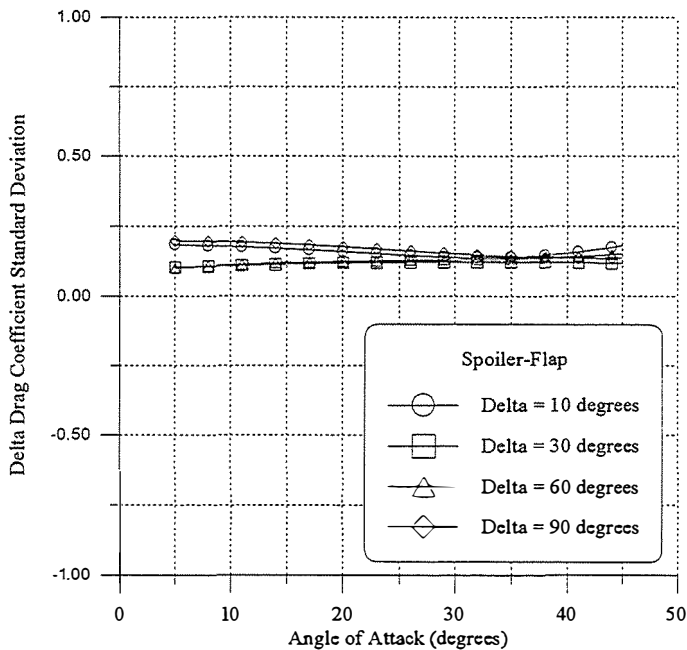


Figure 29. Spoiler-flap ΔC_d uncertainty-analysis results.

Hinge-Moment Results

Figure 30 shows the spoiler-flap hinge-moment data measured for 0, 10, 30, 60, and 90 degree deflections. In summary, the basic three-dimensional trends follow those of the infinite-span wind tunnel data. However, there are notable deviations in the magnitude. Specifically, the finite-span moment coefficient values are, in most cases, slightly lower in magnitude than the infinite-span values.

Vented aileron hinge-moment coefficient data are shown in Figure 31. There are notable differences for all device deflections except 90 degrees, with the magnitude of the finite-span moment coefficients being typically more negative.

Figure 32 shows data for the unvented aileron. There are indications that the hinge-moment measurement apparatus was not operating correctly in all cases. As was noted previously, the tension-compression links used on the unvented aileron proved unreliable. As a result data from these plots should be treated with suspicion.

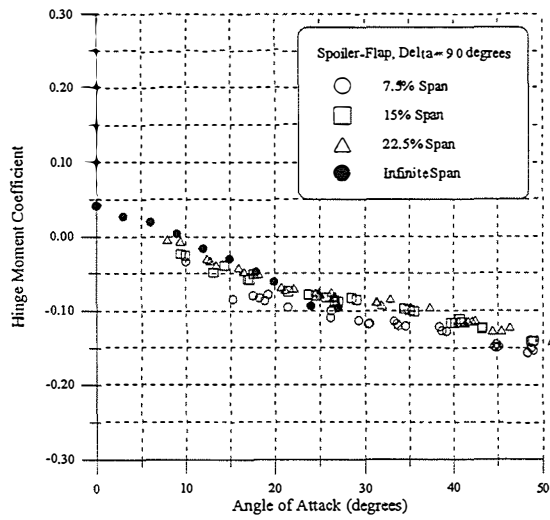
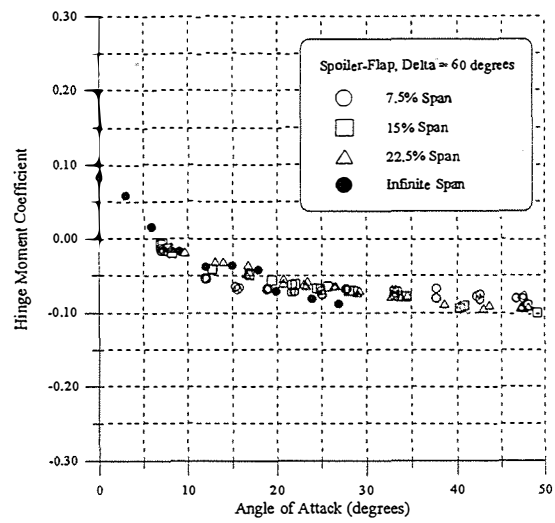
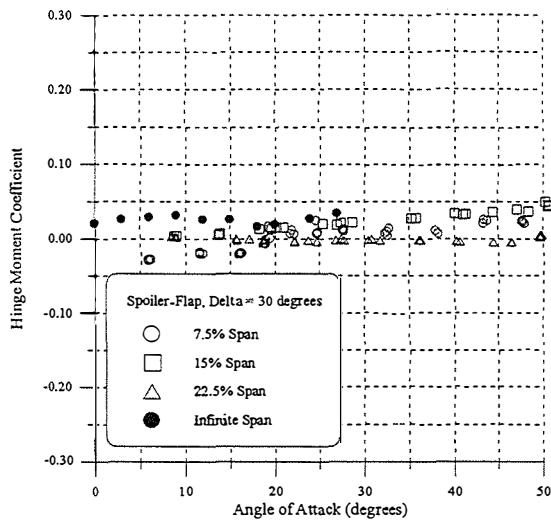
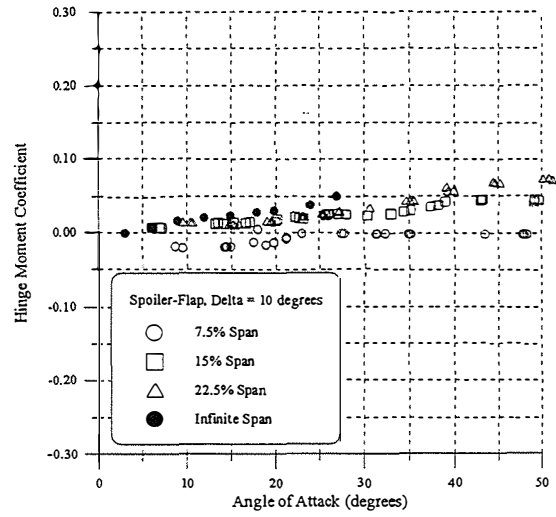
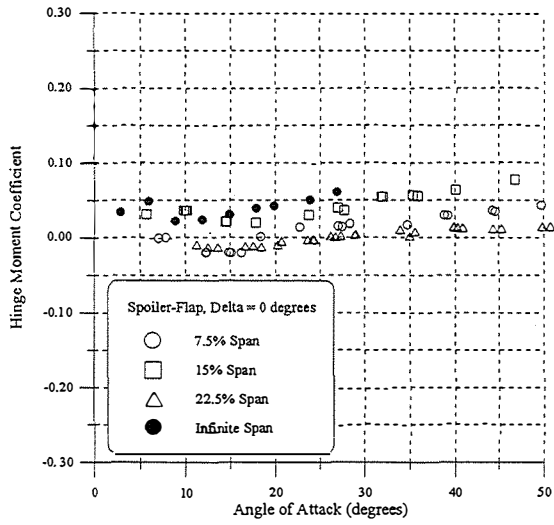


Figure 30. Spoiler-flap hinge-moment coefficient for various spans.

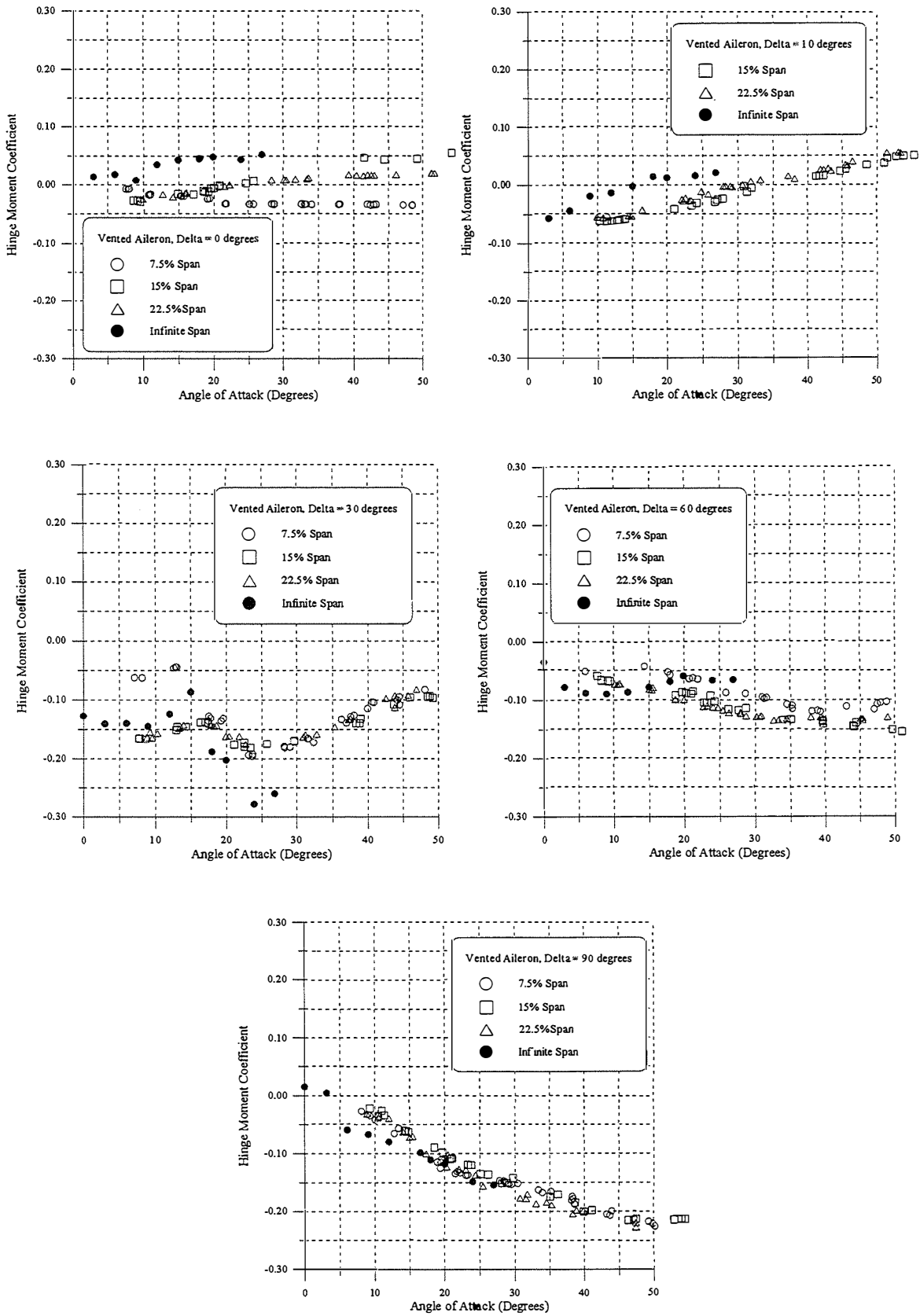


Figure 31. Vented aileron hinge-moment coefficient for various spans.

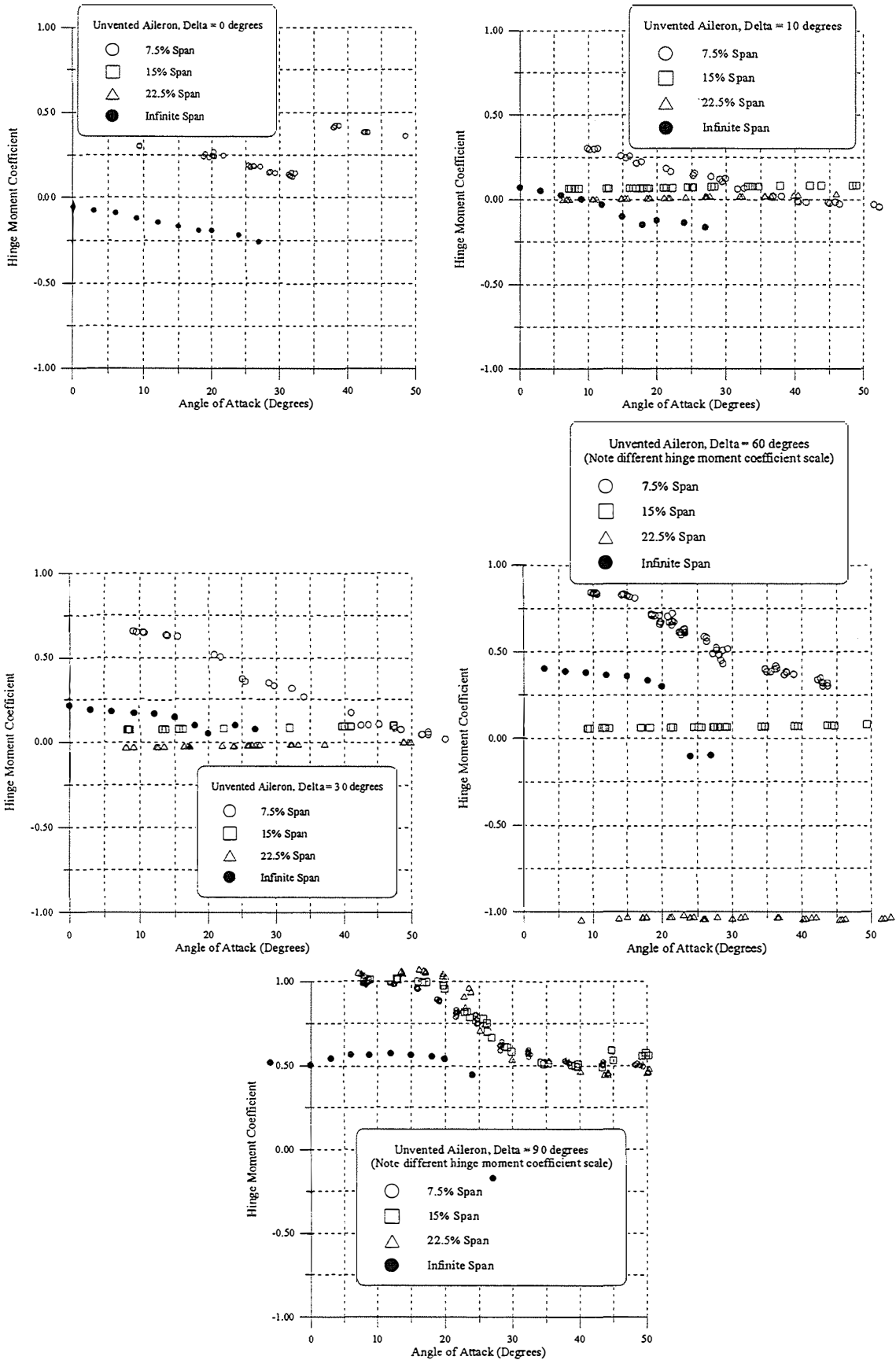


Figure 32. Unvented aileron hinge-moment coefficient for various spans.

Conclusions

Trailing-edge aerodynamic devices were proposed for turbine braking, power modulation, and load alleviation applications. Several wind tunnel tests were performed to evaluate the aerodynamic performance of various configurations. These tests were run almost exclusively for infinite-span geometries. The primary goal of this investigation was to evaluate the performance of finite-span devices in a more representative environment.

A series of atmospheric tests were conducted at the National Renewable Energy Laboratory's National Wind Technology Center using an instrumented turbine, fit with variable-span aerodynamic controls. Three different device configurations (spoiler-flap, vented aileron, and unvented aileron) and spans (7.5%, 15%, and 22.5%) were examined. Comprehensive turbine and atmospheric measurements were used to identify effective changes in the suction, lift, drag, and hinge-moment coefficients as a function of angle of attack and device deflection. The atmospheric tests were conducted at a chord Reynolds number of approximately 1.0 million.

As a result of the investigation, the following conclusions are offered.

- 1) The most pronounced lift-behavior differences between the atmospheric and wind tunnel test data were for angles of attack around stall. Changes in the finite-span lift coefficient data were more constant in comparison to the infinite-span data. This effect on the stall behavior is likely a direct consequence of having a device of lower aspect ratio.
- 2) For device spans greater than 15%, the differences in lift coefficient behavior relative to the infinite-span data are typically small except for the stall region, as was noted above. Results for the shortest span (i.e., 7.5%) devices appear to be influenced by inboard blade and shed-vortex-induced velocity effects.
- 3) Drag differences, as a function of span, appear to follow aspect-ratio trends noted for similar geometries (i.e., flat plates and cylinders). The smallest drag changes occur for devices of the shortest span. The drag increments for devices of spans greater than 15% appear similar in magnitude and are approximately 70% of the infinite-span values. A simple model predicting the drag increment of a finite-span device, as a function of aspect ratio, is offered.
- 4) The unvented aileron lift and drag behavior appears less affected as a result of finite-span. This result suggests that the openings, or vents, associated with the spoiler-flap and vented aileron geometry have an impact on the three-dimensional character of the flow field.
- 5) Hinge-moment coefficient trends, as a function of angle of attack and device deflection, were similar for the infinite- and finite-span configurations. In many cases, the finite-span coefficients had slightly lower magnitudes.

References

- Butterfield, C.P.; Musial, W.P.; Simms, D.A. (1992). *Combined Experiment Phase I: Final Report*. NREL/TP-257-4655. Golden, CO: National Renewable Energy Laboratory.
- Griffin, D.A. (1997). *Investigation of Aerodynamic Braking Devices for Wind-Turbine Applications*. NREL/SR-440-22253. Golden, CO: National Renewable Energy Laboratory.
- Hoerner, S.F. (1958). *Fluid-Dynamic Drag*. Published by the author.
- Holman, J.P. (1994). *Experimental Methods for Engineers. (Uncertainty Analysis)* New York: McGraw-Hill, Inc.; pp. 49-50.
- Quandt, G.A. (1994). *Wind Turbine Trailing-Edge Aerodynamic Brake Design*. Subcontract Report No. TAD-3-12400. Golden, CO: National Renewable Energy Laboratory.
- McCarty, J. (1993). *PROP 93*. West Texas A&M University: Alternative Energy Institute.
- Miller, L.S. (1995). *Experimental Investigation of Aerodynamic Devices for Wind Turbine Rotational Speed Control: Phase I*. NREL/TP-441-6913. Golden, CO: National Renewable Energy Laboratory. Work performed by the Wichita State University National Institute for Aviation Research, Wichita, Kansas.
- Miller, L.S. (1996). *Experimental Investigation of Aerodynamic Devices for Wind Turbine Rotational Speed Control: Phase II*. NREL/TP-441-20507. Golden, CO: National Renewable Energy Laboratory. Work performed by the Wichita State University National Institute for Aviation Research, Wichita, Kansas.
- Miller, L.S.; Migliore, P.G.; Quandt, Q.A. (November 1996). "An Evaluation of Several Wind Turbine Trailing-Edge Aerodynamic Brakes." *ASME Journal of Solar Energy Engineering*; pp. 198-203.
- Prouty, R.W. (1988). *More Helicopter Aerodynamics. (Fly-by-Wire and Smart Control Systems)* Peoria, Illinois: PJS Publications; pp. 73-78.
- Ramsay, R.R.; Janiszewska, J.M.; Gregorek, G.M.. *Wind Tunnel Testing of Three S809 Aileron Configurations for use on Horizontal Axis Wind Turbines*. [Publication number and exact date of publication pending].
- Seddon, J. (1990). *Basic Helicopter Aerodynamics. (Higher Harmonic Control)* Washington, D.C.: AIAA Education Series; pp. 87-88.
- Taylor, J.W.R., ed. (1974). *Jane's All the Worlds Aircraft. (Rockwell International B-1 Bomber Low-Altitude Ride Control System)* New York: Franklin Watts, Inc.; p. 440.

REPORT DOCUMENTATION PAGE

Form Approved
OMB NO. 0704-0188

Public reporting burden for this collection of information is estimated to average 1 hour per response, including the time for reviewing instructions, searching existing data sources, gathering and maintaining the data needed, and completing and reviewing the collection of information. Send comments regarding this burden estimate or any other aspect of this collection of information, including suggestions for reducing this burden, to Washington Headquarters Services, Directorate for Information Operations and Reports, 1215 Jefferson Davis Highway, Suite 1204, Arlington, VA 22202-4302, and to the Office of Management and Budget, Paperwork Reduction Project (0704-0188), Washington, DC 20503.

1.		2. REPORT DATE January 1998		3. REPORT TYPE AND DATES COVERED Subcontractor Report	
4. TITLE AND SUBTITLE Atmospheric Tests of Trailing-Edge Aerodynamic Devices				5. FUNDING NUMBERS C: XAX-5-15217-01 TA: WE803010	
6. AUTHOR(S) L.S. Miller, G.A. Quandt, S. Huang					
7. PERFORMING ORGANIZATION NAME(S) AND ADDRESS(ES) Wichita State University Aerospace Engineering Dept. 1845 N. Fairmount Wichita, Kansas 67260-0044				8. PERFORMING ORGANIZATION REPORT NUMBER	
9. SPONSORING/MONITORING AGENCY NAME(S) AND ADDRESS(ES) National Renewable Energy Laboratory 1617 Cole Blvd. Golden, CO 80401-3393				10. SPONSORING/MONITORING AGENCY REPORT NUMBER SR-500-22350	
11. SUPPLEMENTARY NOTES NREL Technical Monitor: Paul Migliore					
12a. DISTRIBUTION/AVAILABILITY STATEMENT National Technical Information Service U.S. Department of Commerce 5285 Port Royal Road Springfield, VA 22161				12b. DISTRIBUTION CODE UC-1213	
13. ABSTRACT (<i>Maximum 200 words</i>) An experiment was conducted at the National Renewable Energy Laboratory's National Wind Technology Center using an instrumented horizontal-axis wind turbine that incorporated variable-span, trailing-edge aerodynamic brakes. The goal of the investigation was to directly compare results with (infinite-span) wind tunnel data and to provide information on how to account for device span effects during turbine design or analysis. Comprehensive measurements were used to define effective changes in the aerodynamic and hinge-moment coefficients, as a function of angle of attack and control deflection, for three device spans and configurations. Differences in the lift and drag behavior are most pronounced near stall and for device spans of less than 15%. Drag performance is affected only minimally for 15% or larger span devices. Interestingly, aerodynamic controls with vents or openings appear most affected by span reductions and three-dimensional flow.					
14. SUBJECT TERMS renewable energy; wind energy; wind turbines—electricity generation; aerodynamic devices; aerodynamic controls; wind turbine design; wind turbine rotor				15. NUMBER OF PAGES	
				16. PRICE CODE	
17. SECURITY CLASSIFICATION OF REPORT Unclassified	18. SECURITY CLASSIFICATION OF THIS PAGE Unclassified	19. SECURITY CLASSIFICATION OF ABSTRACT Unclassified	20. LIMITATION OF ABSTRACT UL		